Activation of the plant mevalonate pathway by extracellular ATP

Sung-Hwan Cho
University of Missouri-Columbia https://orcid.org/0000-0003-2230-2037
Katalin Tóth
University of Missouri
Daewon Kim
University of Missouri https://orcid.org/0000-0001-5669-1451
Phuc Vo
University of Missouri
Chung-Ho Lin
University of Missouri
Pubudu Handakumbura
Environmental Molecular Sciences Laboratory
Albert Rivas-Ubach
Pacific Northwest National Laboratory
Sterling Evans
University of Missouri
Ljiljana Pasa-Tolic
Pacific Northwest National Laboratory https://orcid.org/0000-0001-9853-5457
Gary Stacey (staceyg@missouri.edu)
University of Missouri https://orcid.org/0000-0001-5914-2247

Article

Keywords: P2K1, extracellular ATP, purinergic signaling, mevalonate (MVA) pathway, mevalonate kinase, mevalonic acid-5-phosphate, innate immunity

Posted Date: August 28th, 2020

DOI: https://doi.org/10.21203/rs.3.rs-61470/v1

Version of Record: A version of this preprint was published at Nature Communications on January 21st, 2022. See the published version at https://doi.org/10.1038/s41467-022-28150-w.

Abstract

The mevalonate (MVA) pathway plays a critical role in multiple cellular processes in both animals and plants. In plants, the products of this pathway impact growth and development, as well as the response to environmental stress. A forward genetic screen of *Arabidopsis thaliana* using Ca^{2+} imaging identified mevalonate kinase (MVK) as a critical component of plant purinergic signaling. MVK interacts directly with the plant extracellular ATP (eATP) receptor P2K1 and is phosphorylated by P2K1 in response to eATP. Mutation of P2K1-mediated phosphorylation sites in MVK eliminates the ATP-induced cytoplasmic calcium response, MVK enzymatic activity, and suppresses pathogen defense. The data demonstrate that the plasma membrane associated P2K1 directly impacts plant cellular metabolism by phosphorylation of MVK, a key enzyme in the mevalonate pathway. The results underline the importance of purinergic signaling in plants and the ability of eATP to influence the activity of a key metabolite pathway with global effects on plant metabolism.

Introduction

All living organisms produce isoprenoids and their diverse derivatives, which are essential for various cellular functions, through the mevalonate (MVA) pathway. In mammals, proper inhibition of 3-hydroxyl-3-methylglutaryl co-enzyme A reductase (HMGR) early in the mevalonate pathway is prescribed as a key treatment for hypercholesterolemia and cardiovascular disease[1–3]. Loss-of-function mutations in mevalonate kinase (MVK) cause two types of inflammatory disease, hyper-immunoglobulin D and periodic fever syndrome (HIDS) and mevalonate aciduria (MA)[4, 5]. Specific inhibition of MVK increases oncogenic mutant p53 degradation, promoting suppression of cancer progression[6]. Fluvastatin, a HMGR inhibitor, suppresses the activity of the purinergic receptor P2 × 4 in monocytes through cholesterol depletion[7]. However, there is no evidence in animals for direct action of purinergic signaling on the MVA pathway. Besides the key role in cholesterol biosynthesis, the MVA pathway provides a wide range of compounds that impact diverse physiological functions, including membrane biogenesis, cell growth, and inflammation[2, 3, 8].

In contrast to animals, less is known about the regulation of the MVA pathway in plants, although it clearly contributes to a wide range of cellular processes. As sessile organisms, plants must be able to grow in place and adapt to a variety of stresses brought about by pests, pathogens or changing environmental conditions. A large number of isoprenoids in the MVA pathway play important roles as mediators of interactions between plants and their environment, such as defense responses against biotic and abiotic stresses. Isopentenyl diphosphate (IPP), a universal precursor of isoprenoids, is used for biosynthesis of phytosterols and dolichols that are essential components of the cell membrane and also the biosynthesis of isoprenoid-derived phytohormones (e.g. abscisic acid, brassinosteroids, gibberellic acid, strigolactones, and cytokinins), which regulate plant growth and development[9–11]. Farnesyl diphosphate (FPP) and geranylgeranyl diphosphate (GGPP) are used for protein prenylation that regulates various processes, such as meristem development, abscisic acid signaling, cytokinin

biosynthesis, and innate immunity[12]. Isoprenes and terpenes, as volatile isoprenoids, are synthesized in plants for protection against pathogens and herbivores, or to communicate with their environment[13]. In addition, other isoprenoids, such as phytosterols and artemisinin, have medical value, including anti-cancer and anti-malaria activities[14, 15]. Hence, the MVA pathway is central to a plethora of cellular processes and, therefore, its regulation is of critical importance.

Several Arabidopsis mutants have been reported with defects in the MVA pathway. The initial reaction is catalyzed by acetoacetyl-CoA thiolase (AACT). While *aact1* mutants have no visible phenotype, RNAi silencing of *aact2* was found to reduce growth and apical dominance, as well as altering the accumulation of sterols[16]. The next enzyme in the pathway, 3-hydroxy-3-methylglutaryl-CoA synthase (HMGS), plays critical roles in organelle development in tapetal cells and pollen coat formation[17]. Two *3-hydroxy-3-methylglutaryl-CoA reductase* (*HMGR*) genes exist in the *Arabidopsis* genome. *hmgr1* mutant plants are male sterile and dwarf, and exhibit early senescence with sterol levels approximately 50% of wild-type[18, 19]. Inhibition of HMGR reduces root growth and the production of key pathway products, such as sterols[20, 21]. No visible phenotypes were observed in single mutants of either *diphospho-MVA decarboxylase* (*MPDC*) *1* or *2*, whereas *mpdc1/2* double mutant plants exhibit ~ 20% unpollinated ovules in the siliques[22]. Mutants lacking isopentenyl diphosphate isomerase (IPPI) 1 and 2 exhibit dwarfism and male sterility, as well as reduced sterol and ubiquinone levels[23]. Loss of farnesyl diphosphate synthase (FPS) activity in *fps1* and *fps2* mutant plants blocks embryogenesis at the early globular stage and reduces sterol and ubiquinone levels[24]. Lack of geranylgeranyl diphosphate synthase (GGPPS) activity prevents embryo development[25]. Surprising given the level of research attention given to the MVA pathway, there are no reports of mevalonate kinase (*mvk*) mutants. Hence, it is unclear what phenotypes would be associated with the loss of this key, early enzyme in the pathway.

Cell surface-localized pattern recognition receptors (PRRs) recognize characteristic microbe or pathogen-associated molecular patterns (MAMPs or PAMPs) and host-derived damage associated patterns (DAMPs), activating pattern-triggered immunity to invading pathogens or pests[26–28]. Extracellular ATP (eATP) is recognized as a DAMP in both plants and animals where it can, for example, be released through cellular damage[26, 29]. The first eATP receptor in plants, P2K1 (also termed DORN1 or LecRK-I.9) binds to ATP and ADP, leading to a variety of cellular changes, among them an increase in cytoplasmic Ca^{2+} levels, production of reactive oxygen species (ROS), and defense-related transcriptional responses[30–33]. Recent studies have begun to unravel the complex signaling events that mediate purinergic signaling in plants but progress is still at an early stage[34]. In order to further elucidate the details of the plant eATP signaling pathway, we performed a forward genetic screen based on the aequorin-bioluminescence Ca^{2+} imaging approach[35]. This resulted in the identification of an *Arabidopsis* mutant that was defective in Ca^{2+} influx triggered upon eATP addition. Subsequent positional cloning and complementation showed that this mutant phenotype was the result of the loss of mevalonate kinase (MVK) function. Subsequent research showed that MVK directly interacts with the eATP receptor P2K1 resulting in transphosphorylation of MVK and subsequent activation of the mevalonate pathway.

These results further underline the ability of purinergic signaling to impact a wide variety of plant processes, similar to its impact on animal physiology.

Results

Cytosolic Ca^{2+} response in 24 − 14 mutant plants upon extracellular ATP treatment

The same genetic screen that ultimately led to the identification of P2K1 as an eATP receptor identified a number of additional mutations that affected the eATP-induced cytoplasmic calcium response, but did not map to the *p2k1* gene[30]. This assay utilized transgenic *Arabidopsis* plants (hereafter ColQ) expressing the calcium reporter protein aequorin[36]. Among the mutants that showed a reduced calcium response to eATP addition was line *24 − 14* (referred to as *mvk-1*) (Fig. 1a,b). Unlike wild-type and *p2k1* mutant plants, mutant line *24 − 14* plants exhibited short roots and small leaves (Supplementary Fig. 2a).

We previously showed that eATP elicits the activation of mitogen-activated protein kinases (MAPKs)[30, 37]. In order to confirm whether the *24 − 14* mutant also failed to trigger eATP induced MAPKs signaling, we checked mitogen-activated protein kinase 3 and 6 (MPK3/6) phosphorylation. Addition of ATP to *24 − 14* mutant plants resulted in a significant decrease in the phosphorylation of MPK3/6 in a manner similar to that found with the eATP receptor mutant *p2k1-3*, while strong activation of MPK3/6 was seen in wild-type plants (Fig. 1c).

The addition of eATP also triggers a strong transcriptional response[30, 31]. Two genes that respond to ATP are *WRKY domain transcription factor 40* (*WRKY40*) and *calcium-dependent protein kinase 28* (*CPK28*). While both of these genes were strongly up-regulated in the wild-type upon eATP elicitation, their expression was only slightly up-regulated in the *24 − 14* mutant (Fig. 1d,e). Thus, with regard to the cellular calcium response, MAPK activation and gene expression, the *24 − 14* mutant line showed clear disruption of normal purinergic signaling.

A mutation in the MVK gene is responsible for the phenotype of the 24 − 14 mutant line

In order to identify the gene responsible for the reduction in purinergic signaling in the *24 − 14* mutant (subsequently referred to as *mvk-1*), we performed map-based cloning and whole-genome Illumina sequencing. These results mapped the *mvk-1* mutation to a 146-kb interval on the short arm of chromosome 5 (Supplementary Fig. 1a,b). Subsequent whole-genome sequencing identified a substitution mutation (G133A; Ala45Ser) in the gene, *At5g24750*, predicted to encode mevalonate kinase (MVK) (Supplementary Fig. 1b,c). This mutation is located at the end of the first exon of *mvk* gene resulting in failure to splice the first intron, as well as a deletion of 28 base-pairs in the *MVK* transcript. In the *mvk-1* mutant, two *mvk* transcripts were observed, whereas no wild-type *MVK* transcript was detected (Supplementary Fig. 2b). These defects lead to premature stop codons (Supplementary Fig. 2c).

In order to characterize the expression patterns of *MVK*, transgenic *Arabidopsis* plants were constructed where the *MVK* gene fused to the β-glucoronidase (*GUS*) reporter gene was expressed from the native

promoter. GUS activity was ubiquitously detected, especially in highly proliferative tissues, including root and shoot apical meristems, as well as in young seedling leaves (Supplementary Fig. 3a-f).

A search of the literature and related databases failed to identify any available *mvk* mutants in *Arabidopsis*[22]. Therefore, in order to verify the observed phenotype of the *mvk-1* mutant, we disrupted the *MVK* gene using CRISPR/Cas9 technology (Supplementary Fig. 4a,b). Consistent with the phenotype of the *mvk-1* mutant line, *mvk*-CRISPR/Cas9 (hereafter *mvk-2*) mutant plants did not show an increase in intracellular calcium concentration upon eATP treatment (Fig. 1a,b; Supplementary Fig. 4c). In addition, expression of *MVK* driven by the *MVK* native promoter or CaMV 35S promoter rescued both the *mvk-1* mutant calcium influx in response to ATP and reduced growth phenotypes (Supplementary Figs. 5a-d and 6a).

Arabidopsis **MVK enzymatic activity**

Previous studies in yeast, fungi, plants, and mammals demonstrated that MVK enzymatically coverts mevalonic acid (MVA) to mevalonic acid-5-phosphate (MVP) at an early step in the MVA pathway (Supplementary Figs. 1d and 2a)[38, 39]. Based on the information of critical conserved motifs in other MVKs from previous studies in human and mosquito, we generated mutated versions of MVK (S149D, D204A) as negative controls[40, 41]. In order to ascertain whether MVK (*At5g24750*) has enzymatic activity, we recombinantly expressed wild-type and mutated versions of MVK fused to a His-tag, and analyzed their enzymatic activity using ultra-performance liquid chromatography (UPLC) (Fig. 2b-d). The enzymatic products of wild-type MVK showed the presence of MVP (~ 6.6 min), identical to standard MVP (~ 6.6 min), whereas no MVP was detected in empty vector control samples, while the MVK-S149D and D204A MVK proteins showed very weak MVP production (Fig. 2c).

mvk-1 **mutant plants show a strong alteration in the level of metabolites derived from the MVA pathway**

Loss of MVK activity in mammals leads to accumulation of MVA and deficiency in downstream compounds for which MVA serves as a precursor[42]. Due to the changes in downstream compounds in the MVA pathway, *Arabidopsis* mutants in this pathway show various physiological phenotypes, such as dwarfism, gametophytic male sterility, small leaves, shorter hypocotyl and roots[16, 17, 19, 23]. It was also shown that application of the HMGR inhibitor, lovastatin, inhibits plant growth[20]. Therefore, one would predict that mutation of *MVK* should strongly alter the levels of downstream MVA pathway metabolites. In order to confirm this prediction, we performed comparative metabolomic analysis of wild-type and *mvk-1* mutant roots harvested from 14-day-old seedlings. As expected, the *mvk-1* mutant plants showed a marked reduction in MVP levels (Fig. 3b), while MVA, a precursor compound of MVP, was significantly higher in the mutant (Fig. 3a). The levels of key downstream metabolites, such as Isopentenyl diphosphate (IPP) and geranylgeranyl diphosphate (GGPP), were also significantly reduced in the *mvk-1* mutant plants (Fig. 3c,d). A full list of the metabolites detected in our analysis is shown in Supplementary Table 1.

If the lack of MVP was solely responsible for phenotypes seen in the *mvk-1* mutants (Fig. 1; Supplementary Fig. 2a), then it might be possible to reverse these phenotypes by simply feeding the plants with MVP. Therefore, we first tested the growth response of the *mvk-1* mutants on MS medium supplemented with 100 µM MVP. The growth of *mvk-1* mutant plants was partially rescued by exogenous application of MVP, demonstrated by seedling growth and also leaf fresh weight (Fig. 3e,f). We hypothesized that if output compounds of the MVA pathway are associated with eATP signaling, application or blocking of the MVA pathway would cause alterations in the ATP-induced calcium response. Indeed, *mvk-1* seedlings, pre-treated with MVP for 1 hour and subsequently treated with ATP, were partially rescued with regard to the eATP-induced cytoplasmic calcium response (Supplementary Fig. 6b,c).

As mentioned previously, lovastatin is an inhibitor of HMG-CoA reductase (HMGR)[1, 20]. Therefore, we treated seedlings for 1 hour with lovastatin and subsequently challenged with eATP. The application of lovastatin strongly reduced the eATP-induced cytoplasmic calcium response in wild-type but not in *mvk-1* plants (Supplementary Fig. 6d,e). Together, these results suggest that metabolites downstream of MVK and HMGR modulate the cellular calcium response to eATP and that this effect, and not some indirect response, is what determines the observed phenotype of the *mvk-1* mutant plants.

MVK is involved in the ATP signaling pathway

The plant eATP receptor P2K1 displays higher preference for purine nucleotides than pyrimidine nucleotides[30]. Therefore, to see whether *mvk-1* mutants show a specific response to purine nucleotides, we checked the calcium response of *mvk-1* mutant plants to a variety of nucleotides. Both *mvk-1* and *mvk-2* mutant plants exhibited defects in the cytoplasmic calcium response to purine nucleotides, such as poorly hydrolyzed ATP analogs (ATPgS and ADPbS), ADP, GTP, and ITP, whereas the *mvk-1* and *mvk-2* mutants responded poorly to pyrimidine nucleotides, CTP, TTP, and UTP, similar to wild-type plants (Fig. 4a,b). We also tested the nucleotide induced calcium responses in *Arabidopsis* wild-type plants ectopically expressing *MVK* driven by the strong CaMV 35S promoter (*p35S::MVK*). The *p35S::MVK* lines showed ~30% higher calcium influx than wild-type plants in response to ATP (Supplementary Fig. 5e,f). The intracellular calcium responses of the *mvk-1* mutants to various biotic (flg22, chitin, elf26, and pep1) and abiotic (cold water, NaCl, D-glucose, and mannitol) calcium elicitors were similar to those of wild-type plants (Fig. 4c,d). Consistent with these results, *mvk-2* mutant plants were also non-responsive to the same elicitors (Fig. 4c,d). Overall, our results suggest that *MVK* plays an important role in the response to purine nucleotides, likely mediated through the action of the P2K1 receptor.

As previously shown, eATP treatment and wounding induce overlapping transcriptional responses[30]. Therefore, we tested whether both eATP and wounding induce expression of *MVK*. Indeed, we found that *MVK* expression was induced by eATP over a time-course and also by wounding of plants, as measured by *pMVK::GUS* expression (Supplementary Fig. 3g,h).

MVK interacts with P2K1 *in planta*

Unlike the eATP receptor P2K1, which localizes to the plasma membrane[43], MVK is predicted to localize in the cytosol (SUBA; http://suba.plantenergy.uwa.edu.au)[22]. When we expressed a YFP fluorophore tagged version of MVK in protoplasts, MVK was confined to the cytosol (Fig. 5c). Therefore, if MVK plays a role in eATP signaling pathway, it could be via direct interaction with the eATP receptor. In order to test this hypothesis, we co-expressed HA-tagged P2K1 in *Nicotiana benthamiana* leaves with a Myc-tagged MVK with or without the addition of ATP (Fig. 5a). Subsequent co-immunoprecipitation (Co-IP) showed a clear interaction of MVK and P2K1 that was enhanced by eATP. Similarly, use of the split-luciferase complementation imaging (LCI) assay in *N. benthamiana* leaves also showed interaction between MVK and P2K1, which was enhanced by eATP (Fig. 5b). The biomolecular fluorescence complementation (BiFC) assay in *Arabidopsis* protoplasts also showed that MVK specifically interacts with P2K1 on the plasma membrane (Fig. 5d). The cytoplasmic kinase, mitogen-activated protein kinase kinase 3 (MKK3)[44], was used as a negative control in these assays and showed no interaction with P2K1 (Fig. 5). Together, the results suggest that MVK directly interacts with P2K1 receptor on the plasma membrane and that this interaction is strengthen by the addition of eATP.

MVK is phosphorylated by P2K1

It was previously demonstrated that the kinase activity of P2K1 is essential for purinergic signaling *in planta*[30, 33]. Therefore, we tested whether P2K1 can phosphorylate MVK. Full-length MVK protein, the P2K1 kinase domain (P2K1-KD) or a P2K1 kinase-dead version (P2K1-1-KD) were recombinantly expressed and purified. Recombinant MVK protein was incubated with the purified P2K1-KD and P2K1-1-KD and assayed for phosphorylation by radiolabeling with g-[32P]-ATP. The results show that the purified P2K1 kinase domain (KD) strongly trans-phosphorylated MVK *in vitro*, whereas the kinase-dead version of GST-P2K1-1-KD failed to phosphorylate MVK (Fig. 6a).

Mass spectrometric analysis of in-solution-trypsin digested peptides identified 13 possible *in vitro* MVK sites phosphorylated by P2K1 (Supplementary Fig. 7). MVK is composed of three domains, the Galacto, Homoserine, Mevalonate, and Phosphomevalonate (GHMP) kinase N- and C-terminal, and the ATP binding domain (Supplementary Fig. 7). In the GHMP kinase N-terminal region of MVK, two sites targeted by P2K1 were identified (T169, S208), and three sites (S329, T332, T342) were identified in the GHMP kinase C-terminal region, while eight other sites (S77, S78, T79, S87, S89, T222, S263, T285) were identified outside of GHMP domains (Supplementary Fig. 7). In order to test whether the identified phosphorylated sites in MVK are important for activity or regulation of this enzyme, the 13 phospho-residues were each substituted with alanine to eliminate the possibility of trans-phosphorylation. Subsequent assays showed that, of these 13 residues, proteins having the MVK-S87A, S89A, T285A, S329A, or T342A mutation showed reduced phosphorylation in the presence of P2K1 (Fig. 6b). In order to investigate the relevance of this phosphorylation to MVK-mediated cytoplasmic calcium influx in response to ATP, wild-type MVK, as well as the S87A, S89A, T285A, S329A, or T342A MVK proteins were each fused to the HA epitope tag and, subsequently ectopically expressed in *mvk-1* mutant plants. Plants expressing the phospho-null S87A or S89A MVK proteins showed partial complementation of the ATP-induced cytoplasmic response upon addition of eATP. Plants expressing either S329A or T342A MVK

proteins showed no complementation (Fig. 6c). Expression of the T285A MVK protein fully restored the wild-type phenotype (Fig. 6c). From this analysis, we conclude that phosphorylation of S329A and/or T342A is critical for MVK function. Note that in every case, western blotting showed strong and roughly similar expression of the recombinant proteins (Fig. 6c).

In order to further confirm whether P2K1-mediated MVK phosphorylation affects MVK enzymatic activity, we combined the recombinant proteins *in vitro* and then measured MVK enzymatic activity (Fig. 6d,e). Production of MVP was significantly higher when MVK-WT-HIS was in the presence of GST-P2K1-KD, relative to similar experiments performed with the kinase-dead version of GST-P2K1-1-KD (Fig. 6e). Production of MVP by MVK-S329A-HIS or MVK-S342A-HIS in the presence of either GST-P2K1-KD or GST-P2K1-1-KD was significantly lower relative to experiments performed with the wild-type MVK protein (Fig. 6e). Overall, these results suggest that MVK is a direct phosphorylation target of P2K1, and S329 and T342 are the critical MVK residues directly phosphorylated by P2K1 that modulate enzymatic activity.

P2K1-mediated MVK phosphorylation plays an essential role in plant innate immunity

Activation of MAPK signaling is a critical aspect of the pathogen response pathway[45]. Previous studies reported that the P2K1 receptor is involved in plant defense against pathogens[33, 46-50]. *Arabidopsis* responds to eATP with activation of MAPK phosphorylation[30]. In addition, application of eATP led to enhanced resistance to the bacterial pathogen *Pseudomonas syringae* via P2K1 signaling[33]. Given that the reduced activation of MPK3/6 in the *mvk-1* mutant background (Fig. 1c) and the interaction between MVK and P2K1 (Fig. 5), it seemed likely that MVK activation by P2K1 would also play a role in the plant innate immune response.

To investigate the involvement of MVK in plant innate immunity, we challenged plants with the pathogen *P. syringae* DC3000 lux. Arabidopsis *salicylic acid induction-deficient 2* (*sid2*) mutant plants were used as a susceptible control[51]. As predicted, these experiments showed that *mvk-1* mutant plants were more susceptible to the bacterial pathogen than wild-type plants (Fig. 7a). Consistent with the bio-luminescence assay, direct bacterial counts also confirmed higher pathogen numbers on *mvk-1* mutant plants relative to wild-type plants (Fig. 7b). In order to further understand whether the phosphor-null mutants S329A and T342A exhibit susceptible innate immunity, we also challenged these mutant plants with *P. syringae*. Both phosphor-null mutants were susceptible to the bacterial pathogen (Fig. 7a). In addition, bacterial growth was significantly increased in the both S329A and T342A mutant plants compared to wild-type (Fig. 7b). These results demonstrate that MVK is associated with P2K1 mediated innate immunity in *Arabidopsis*.

Plants perceive a change in isoprenoids by down-regulation of *farnesyl diphosphate synthase* (*FPS*) in the MVA pathway (Supplementary Fig. 1d) as a stress signal, leading to misregulation of genes involved in abiotic and biotic stress responses, which affects the level of metabolites related to wounding and/or stress response [e.g., jasmonic acid (JA), and salicylic acid (SA)][52]. SA is known for its role in initiating defense responses against pathogens such as *P. syringae*[53]. Given that *mvk-1* plants showed reduced

levels of IPP and GGPP (Fig. 3c,d), it seemed possible that increased pathogen susceptibility in *mvk-1* plants is due to defects in SA accumulation or biosynthesis. To better understand how MVK contributes to bacterial pathogen resistance, we performed metabolomic analysis of 2-week-old wild-type and *mvk-1* mutant plant roots. We found that SA was reduced in *mvk-1* mutant plants (Fig. 7c). Benzoic acid, a direct precursor of salicylic acid, was strongly reduced in *mvk-1* mutant plants (Fig. 7d). In contrast, JA levels were slightly higher in *mvk-1* mutant plants (Fig. 7e). We conclude that this observed reduction in SA levels likely contributes to the increased susceptibility of *mvk-1* mutant plants to *P. syringae* DC3000.

In addition, to gain insight into whether eATP could affect the expression of *FPS*, we re-examined the previously published transcriptome data comparing ATP-treated wild-type and *p2k1* plants[30]. Interestingly, these data showed that *FPS1* transcript levels in wild-type plants were reduced in response to ATP compared to mock treated plants. However, no statistical difference in the level of *FPS1* was observed in *p2k1* mutant plants compared to mock-treated wild-type plants[30]. To confirm these observations, we directly measured *FPS1* expression in wild-type, *mvk-1*, and *p2k1-3* plants with or without ATP treatment. Indeed, after ATP treatment, *FPS1* expression in wild-type plants was significantly reduced compared to wild-type mock-treated plants, whereas no difference in expression was observed in *mvk-1* mutants compared to *mvk-1* mock-treated plants (Fig. 7f). The level of *FPS1* was slightly reduced in *p2k1-3* plants after addition of ATP compared to *p2k1-3* mock-treated plants (Fig. 7f). These results suggest that eATP, as a danger signal, participates in the expression of *FPS1* via *MVK*, likely through the direct action of P2K1 on MVK enzymatic activity.

Discussion

Both in animals and plants, various intermediates and metabolites derived from the MVA pathway are known to play critical roles, including sterol synthesis, growth, defense response, and development[2, 54]. Given that the products derived from the mevalonate pathway are extremely diverse including cellular signaling compounds[54, 55], it is not surprising that this pathway would be subject to tight regulation, including the ability to respond to changing environmental conditions, including abiotic and biotic stress. In general, plant plasma-membrane localized receptor-like kinases (RLK), modulate cellular metabolism indirectly, commonly through action on cytoplasmic kinases that subsequently impact various metabolic pathways[56]. Thus, it is somewhat unusual that P2K1 should directly modulate MVA pathway activity through direct interaction and phosphorylation of MVK. However, there is precedence for such a model. Specifically, previous research showed that the plasma membrane RLK NORK (also called MtDMI2 or LjSYMRK) directly regulates the MVA pathway via interaction with HMGR[55, 57], which impacts the cytoplasmic calcium response known to be critical to legume nodulation. At present, the cognate ligand for DMI2 receptor is unknown. Given that previous research has shown that purine nucleotides can promote legume nodulation[58], it is intriguing to postulate that eATP is also playing a role in legumes through modulation of MVA activity.

Eukaryotic *MVK* genes have been studied in yeast, ginkgo, rat and human[59–62]. In particular, human MVK has been well studied in relation to auto-immune diseases such as mevalonate kinase deficiency (MKD), and this led to the development and discovery of important drugs, such as anakinra and canakinumab[4–6]. Approximately 80 *MVK* genetic mutations are known to be associated with MKD disease[63]. However, surprisingly given the number of MVA pathway mutants available in *Arabidopsis*[22], to our knowledge, no plant *mvk* mutants have been characterized previously.

Previous research clearly indicates that eATP is an important stress signaling compound in plants, which in *Arabidopsis* is recognized by the P2K1 receptor, perhaps in combination with the recently identified, closely related P2K2 receptor[34]. Details of importance of eATP signaling in plants are emerging, including evidence that P2K1 contributes to plant defense against pathogens[33, 48, 49], ATP mediated ROS signaling, JA levels and S-acylation[33, 37, 49]. We can now add to this list the ability of P2K1 to directly alter plant metabolism by regulation of MVK.

Identification of MVK as an interacting partner with P2K1 receptor is fundamentally important for understanding how plants modulate metabolomic pathways through the RLK-triggered signaling pathway. Unlike the early secondary signaling messengers (Ca^{2+}, ROS), it may be necessary to go through several signaling steps to regulate metabolism. Tripathi *et al*. showed that ATP treatment did not affect SA levels at an early time point, but showed that eATP did induce some SA-dependent genes[49]. Another study showed that ATP reduced SA levels at a later time point[64]. These latter results are consistent with our findings that ATP reduced SA levels, which we attribute to modulation of MVA pathway activity.

As mentioned above, research in *M. truncatula* showed that HMGR activity in the MVA pathway was essential for the ability of the invading rhizobium to induce the calcium oscillations necessary for successful nodulation[55]. This work is fully consistent with the results presented here showing a key role of the MVA pathway of mediating the cytoplasmic calcium response to elicitation, be it via eATP, rhizobia or pathogens. The question then is how does this metabolic pathway impact cellular responses that originate very quickly at the plasma membrane via the action of various RLKs. Current results do not provide a ready explanation for these observations. However, as a working hypothesis, it seems reasonable that reduction of the key MVA metabolic intermediates, FPP and GGPP, involved in membrane anchoring of a variety of proteins, including receptors[12, 65], could drastically affect the overall environmental response of plants to any number of factors.

In conclusion, we identified Arabidopsis MVK as a direct phosphorylation target of P2K1, which results in activation of the MVA pathway in response to eATP elicitation, resulting in a variety of metabolic changes in the plant (Fig. 7g). Understanding this particular connection between purine signaling and the MVA pathway may ultimately provide potential molecular genetic targets for engineering crops with increased beneficial metabolites, or enhanced yield or improved stress resistance. The results also add to a growing body of evidence that purinergic signaling is as central in plants as it is in animals.

Methods

Plant materials and growth conditions. Wild-type aequorin-expressing transgenic *Arabidopsis* ColQ (Col-0 background) plants were kindly provided by Marc Knight[36]. The EMS-induced mutant population was described previously[30]. The *24 – 14* (subsequently referred to as *mvk-1*) mutant was backcrossed with the ColQ aequorin transgenic line three times (BC3F3). This backcrossed line was then used for phenotyping. Arabidopsis seeds were sown onto half strength Murashige and Skoog (MS) medium containing 1% (w/v) sucrose, 0.5% (w/v) phytagel, and 0.05% (w/v) MES pH 5.7. After 4 °C cold treatment for three days, the plates were placed vertically in a growth chamber (16 h light/8 h dark cycle, 22 °C, 100 µE $cm^{-2}sec^{-1}$ light intensity). For other experiments, 10-day-old seedlings or 3-week-old plants were grown in PRO-MIX soil (Premier Tech Horticulture) in a growth chamber (16 h light/8 h dark cycle, 22 °C, 70% humidity and 150 µE $cm^{-2}sec^{-1}$ light intensity).

Plasmid constructs and plant/protoplast transformation. Full-length *MVK* (At5g27450) and *MKK3* (At5g40440) genes were amplified using gene-specific primers (Supplementary Table 2) and cDNA derived from wild-type plants. The PCR products were cloned into pDONR-Zeo (Invitrogen) or CloneJET (Thermo Fisher Scientific) vectors.

For constructs expressing recombinant proteins in *E. coli*, the cDNA of *MVK* and *MKK3* were ligated into pET21a (Novagen) resulting in a His-tag fusion at the C-terminus of the protein. The P2K1 kinase domain and P2K1-1 kinase-dead in pGEX-5X-1 were previously described[30]. For cloning the various restriction enzymes (Supplementary Table 2) and T4 ligase (Promega) were used. MVK-S77A, S78A, T79A, S87A, S89A, T169A, S208A, T222A, S263A, T285A, S329A, T342A, and MKK3-kinase dead clones were generated by site-directed mutagenesis.

For Bimolecular Fluorescence Complementation (BiFC) assay, full-length coding sequences of *MVK*, *P2K1*, and *MKK3* without stop codons were cloned into entry vector pDONR-Zeo and subcloned into pAM-PAT-35S::YFP, pAM-PAT-35S::YFPn, and pAM-PAT-35S::YFPc destination vectors through LR reaction[66].

For co-immunoprecipitation assays in *Nicotiana benthamiana*, full-length CDS of *MVK* and *MKK3* from the pDONR-Zeo vectors were cloned into pGWB17, and full-length CDS of *P2K1* from the pDONR-Zeo vector was cloned into pGWB14 using LR reaction.

To generate constructs for the split-luciferase complementation assay in *N. benthamiana*, full-length CDS of *MVK*, *P2K1*, and *MKK3* from the pDONR-Zeo vectors were cloned into pCAMBIA-GW-Nluc and pCAMBIA-GW-Cluc using LR reaction.

In order to generate stable transgenic Arabidopsis plants, the *MVK* promoter, a 1,350 bp region containing the 5'-UTR and encoding the first 17 amino acids, was cloned into pDONR-Zeo. To generate a fusion to the β-glucuronidase (GUS) reporter gene, the promoter region was subcloned into a plant binary vector pMDC162, generating the reporter construct *pMVK::GUS*.

The MVK promoter fragment (1,350 bp, see above) was fused with the *MVK* gene, followed by cloning into the binary vectors pGWB13 using LR reaction. *MVK* gene mutant clones containing different, mutated phosphorylation sites were generated by site-directed mutagenesis. Those fragments were cloned into the pGWB13 vector using LR reaction. These binary vectors were transformed into *Agrobacterium tumefaciens* GV3101 and used for transformation of *Arabidopsis* plants via the floral dip method[67]. The homozygous T3 lines were screened based on hygromycin resistance.

CRISPR/Cas9 editing was performed as previously described by Schiml et al[68] (http://www.botanik.kit.edu/molbio/940.php). The Cas9 gene (UBQ3-Cas9-SK), driven by the UBQ3 promoter and the chimeric single guide RNA (AtU6–26-SK), driven by the AtU6–26 promoter was obtained from addgene (https://www.addgene.org/crispr/plant/). The *bar* gene, driven by mannopine synthase promoter of the binary vector pFGC5941, was used as a selection marker for *Arabidopsis* transformation. *MVK* specific single-guide RNA sequences were designed using the Zhang lab web-based tool: http://crispor.tefor.net/. Two gRNAs (MVK-253 and MVK-927) were used to create defined deletions within the exon of *MVK* gene. For each gRNA, a pair of DNA oligonucleotides (Supplementary Table 2) was synthesized and annealed to generate dimers. Subsequently, the annealed DNA was cloned using *Bbs*I restriction sites into pAtU6–26-SK to create pSK-AtU6–26-gRNA, and sequence integrity was confirmed by Sanger sequencing (University of Missouri, DNA Core Facility). To obtain a functional Cas9 expression construct for targeted mutagenesis, pSK-AtU6–26-gRNAs were cut with *Eco*RI-*Spe*I, and UBQ3-Cas9-SK was digested with SbfI-SpeI. These 3 fragments were assembled into pFGC5941 by *Eco*RI-*Sbf*I restriction digestion followed by ligation to obtain pFGC5941-AtU6- UBQ3/Cas9 construct. All primers used in this study are listed in Supplementary Table 2.

Cytoplasmic calcium assays. Assays were conducted as previously described[30]. Briefly, 5-day-old seedlings were individually transferred to a single well of a 96-well plate with 50 µl of reconstitution buffer containing 10 µM coelenterazine (NanoLight Technology), 10 mM $CaCl_2$ and 2 mM MES pH 5.7, and incubated overnight at room temperature in the dark. Fifty microliters of nucleotides, abiotic and biotic elicitor treatment solution (double concentration) were applied in each well. The production of luminescence was monitored using an image-intensified CCD camera (Photek 216; Photek, Ltd.). One hundred microliters of discharging buffer containing 2 M $CaCl_2$ and 20% (v/v) ethanol was used to estimate the remaining, unchelated aequorin. Photon counting data were converted into calcium concentration as previously described[36].

EMS mutagenesis and mutant screening. In addition to the various *p2k1* mutants identified previously by screening an EMS-mutagenized library derived from *Arabidopsis thaliana* expressing aequorin[30], an additional 7 mutants were identified whose mutations did not map to the *p2k1* gene. The *mvk-1* mutant line was among these seven, which led to the identification of the *mvk-1* mutant allele by map-based cloning and whole-genome sequencing. The response of the *mvk-1* mutant plants to ATP was tested by applying an increasing concentration (10, 100, 500, and 1000 µM) of ATP. We also tested the *mvk-1* plants for the specificity of their defect by applying a variety of known cytoplasmic calcium

elicitors/treatments (e.g. 100 µM of ATP, ATPγS, ADP, ADPβS, AMP, Adenosine, GTP, ITP, CTP, TTP, and UTP; 100 nM of flg22, chitin, elf26, and pep1; ice-cold water; 5% D-glucose; 300 mM NaCl and mannitol).

Map-based cloning. We generated a mapping population by crossing the *mvk-1* mutant plants with *A. thaliana* Landsberg *erecta* ecotype plants, subsequently using the F2 generation for genotyping. The mutant phenotype was screened by monitoring the ATP-induced calcium response (via aequorin). Genetic mapping placed the *mvk-1* mutation on the short arm of chromosome 5 as measured by co-segregation with the ATP response phenotype. SSR marker nga76 and nga139 on chromosome 5 were strongly linked to the mutant phenotype and additional INDEL markers were used for further mapping. We narrowed the mutant phenotype region in the map to an ~ 146 kb interval between INDEL3576 (two recombinants in 76 F2 populations) and INDEL3630 (one recombinant in 76 F2 populations). All the molecular markers are listed in Supplementary Table 2.

Whole genome sequencing. The *mvk-1* mutant plants were backcrossed three times with wild-type ColQ and homozygous lines (BC3F3) were obtained for whole genome sequencing. As an internal reference, DNA from the ColQ originally used for EMS mutagenesis was also prepared for sequencing. Single leaves from 75 plants (3 weeks-old) were pooled and genomic DNA extraction was performed according to the manufacturer's instructions (Qiagen, DNeasy Plant Mini Kit). The whole genome sequencing was carried out by the DNA Core Facility of the University of Missouri (https://dnacore.missouri.edu/ngs.html). Genomic DNA (3 µg) was sheared to 350 bp and used for DNA PCR-Free library preparation. Sequencing was performed on a Hiseq 2000 (Illumina) instrument with 100 bp single end reads (> 30 × coverage for all DNA samples using 1 × 100 run). Reads were quality trimmed using FASTX FASTQ Quality Trimmomatic version 0.32[69]. Reads were then aligned back to the TAIR10 version of the *Arabidopsis* genome using Bowtie version 2[70]. Sam and output-pileup files were generated using Samtools version 0.1.7[71]. The output-pileup files converted to the NGM emap file in Next generation mapping web tool (http://142.150.215.220/ngm/) and then analyzed single nucleotide polymorphisms as previously described[72].

MAPK phosphorylation assay. Leaf discs from 3-week-old plants were incubated in 2 mM MES pH 5.7 at room temperature overnight. After treatment with 100 µM ATP for 0, 5, 10, 30, and 60 min, total protein was extracted with extraction buffer containing 50 mM Tris-HCl pH 7.5, 150 mM NaCl, 1 mM EDTA, 0.5% Triton-X 100, 1 mM DTT, 0.1 mM PMSF, and 1X protein inhibitor (Pierce) for 1 hour on ice. The extracted total proteins were mix with 5X Laemmli loading buffer containing 10% SDS, 50% glycerol, 0.01% bromophenol blue, 10% beta-mercaptoethanol, 0.3 M Tris-HCl pH 6.8, and heated in boiling water 5 minutes. The total extracted proteins were separated by 10% SDS-PAGE gel and detected by immunoblotting with rabbit anti-phospho-p44/p42 MAPK antibody (Cell signaling technology).

RNA isolation and quantitative real-time (qRT)-PCR. 10-day-old seedling plants were transferred into a 6-well plate and incubated in liquid MS medium in a growth chamber overnight. Samples were collected after treatment with 100 µM ATP, and total RNA was extracted using a RNeasy Plant Mini Kit (Qiagen) according to the manufacturer's instructions. RNA concentration was measured after Turbo DNA-free

DNase (Ambion) treatment, and 1 µg RNA was used for first-strand cDNA synthesis using reverse transcriptase (Promega). The qPCR was performed using the PowerUp™ SYBR Green master mix (Applied Biosystems) following the manufacturer's instructions. For data analysis, Rn data were extracted from ABI 7500 PCR machine and LinReg software (version 11.0) was used to determine Cq data and baseline. Transcript levels were normalized against the expression of the *UBIQUITIN* (*UBQ*) or *SAND* (*At2g28390*) gene. The gene specific primers used are listed in Supplementary Table 2.

MVK enzyme assay. Enzymatic activities were determined by following the procedure described by Reitzle et.al (2015). In brief, 2 µg of purified MVK-HIS protein was incubated with 2 µg GST-P2K1-KD kinase in reaction buffer (10 mM Tris-HCl pH 7.4, 5 mM $MgCl_2$, 2 mM ATP, 100 µM Mevalonic acid). Reactions were kept at 30 °C for 10 minutes, and then terminated by adding an equal volume of acetonitrile. The samples were centrifuged for 20 min at 20,000 rcf and the supernatant was further processed for HPLC-MS/MS analysis. For quantification of mevalonic acid-5-phosphate, 50 µl internal standard working solution (containing 50 µM/L [13C, 2H3]-DL mevalonic acid-5-phosphate) were added to 50 µl enzyme assay sample, calibrator or quality control sample. After vortexing, the samples were evaporated to dryness under a gentle stream of nitrogen. Subsequently, 50 µl butanol–HCl (Sigma-Aldrich) was added to derivatize the carboxy acid group of mevalonic acid-5-phosphate (Sigma-Aldrich) and its internal standard to the corresponding butyl ester at 70 °C for 45 minutes. The samples were centrifuged for 2 minutes at 1500 rcf and evaporated to dryness. The residue was dissolved in 1000 µl water/acetonitrile (1:1) and further diluted 1:100 with water/acetonitrile (1:1). The diluted solution was loaded and analyzed by a Waters Alliance 2695 high Performance liquid chromatography (HPLC) system coupled with Waters Acquity TQ triple quadrupole mass spectrometer (MS/MS). The analytes were separated by a Kinetex C18 (100 mm x 4.6 mm; 2.6 µm particle size) reverse-phase column (Phenomenex). The mobile phase consisted of 10 mM ammonium acetate and 0.1% formic acid in water (A) and 100% acetonitrile (B). The gradient conditions were 0-0.5 min, 2% B; 0.5-7 min, 2–80% B; 7.0–9.0 min, 80–98% B; 9.0–10.0 min, 2% B; 10.0–15.0 min, 2% B at a flow rate of 0.5 ml/min. The ion source in the MS/MS system was electrospray ionization (EI) operated in the negative ion mode $[M-H]^-$ with capillary voltage of 1.5 kV. The ionization sources were programmed at 150 °C and the desolvation temperature was programmed at 450 °C. The MS/MS system was in the multi-reaction monitoring (MRM) mode with the optimized collision energy. The derivatized mevalonate-5-phosphate butyl ester was quantified with mass transition m/z 283◊96.

GUS staining and imaging. For detecting GUS activity, 10-day-old or 3-week-old plants were incubated in histochemical staining buffer (100 mM $NaPO_4$ pH 7.0, 10 mM EDTA, 0.1% Triton X-100, 1 mM $K_3Fe(CN)_6$, 1 mM 5-Bromo-4-chloro-3-indoyl-beta-D-glucuronide) for 6 hours and then washed with 70% EtOH until tissue cleared. For the wounding treatment, rosette leaves were crushed using a hemostat forceps.

Co-immunoprecipitation assay. *Agrobacterium tumefaciens* GV3101 carrying the indicated constructs in infiltration buffer (10 mM MES pH 5.7, 10 mM $MgCl_2$, 150 µM acetosyringone) was infiltrated into 3-week-old leaves of *N. benthamiana*. After 2 days, 200 µM of ATP and 2 mM MES (pH 5.7) were infiltrated into the same leaves. Total protein was extracted from pulverized (ground in liquid nitrogen) *N. benthamiana*

leaf tissues using the following buffer: 50 mM Tris-HCl (pH 7.5), 250 mM NaCl, 10 mM $MgCl_2$, 1 mM EDTA, 1 mM DTT, 0.2 mM PMSF, 10% glycerol, 0.5% Triton-X 100, and 1X protease inhibitor (Thermo Fisher Scientific) by gentle rotation at 4 °C for 2 hours. The solution was centrifuged at 20,000 g for 10 minutes at 4 °C. The supernatant was transferred into a new tube and 1 µg anti-Myc (Sigma-Aldrich) was added, and incubated overnight with end-to-end shaking at 4 °C. Subsequently, 25 µl protein A resin (GenScript) was added for 4 hours, spun down and washed five times with washing buffer containing 50 mM Tris-HCl pH 7.5, 150 mM NaCl, and 1X protease inhibitor. After washing, the resin was eluted with 50 µl 1X SDS-PAGE loading buffer and the eluent heated in boiling water for 10 minutes. The proteins were separated by 10% SDS-PAGE gel electrophoresis and detected by immunoblotting with anti-HA-HRP (Sigma-Aldrich; dilution, 1:1000).

Split-luciferase complementation imaging assay. *Agrobacterium tumefaciens* GV3101 containing the indicated constructs were incubated in infiltration buffer (10 mM MES pH 5.7, 10 mM $MgCl_2$, 150 µM acetosyringone) for 2 hours in dark and subsequently used to infiltrate into 3-week-old leaves of *N. benthamiana* for 2 days before the LUC activity measurement. 1 mM D-luciferin (Goldbio) was sprayed 1 time onto the leaves, and then kept in the dark for 7 minutes to allow the chlorophyll luminescence to decay, the luminescence was monitored using a CCD camera (Photek 216; Photek, Ltd.).

Bimolecular fluorescence complementation assay. The subcloned YFP protein fusion constructs were co-transformed into *Arabidopsis* protoplasts by polyethylene glycol (Sigma-Aldrich) for transient expression[73] and then incubated in a 23 °C chamber overnight in the dark. The fluorescence signals were monitored using a Leica DM 550B Compound microscope with Leica DFC290 color digital camera. FM 4–64 dye (Fisher scientific) was used to stain the plasma membrane for reference.

In vitro kinase assay. 2 µg of purified GST, GST-P2K1-KD or GST-P2K1-1-KD kinase was incubated with 1 µg MVK-HIS (WT, S77A, S78A, T79A, S87A, S89A, T169A, S208A, T222A, S263A, T285A, S329A, T332A, and T342A) as substrate in a 20 µl reaction buffer (20 mM Tris-HCl pH 7.5, 10 mM $MgCl_2$, 5 mM EGTA, 100 mM NaCl, and 1 mM DTT, 2 mM ATP, and 10 µCi radioactive [γ-^{32}P] ATP) for 1 hour at 30 °C. The reaction was stopped by boiling for 5 minutes with 5x SDS loading buffer. After electrophoresis in 12% SDS-PAGE, the gel was exposed for 12 hours for autoradiography. The proteins within the gel were visualized with coomassie brilliant blue. Myelin basic protein (MBP) (Sigma), GST, and MKK3-KD were used as controls. Experiments were repeated independently three times.

MVK phosphorylation site identification by LC-MS/MS. 20 µg of purified GST-P2K1-KD kinase was incubated with 10 µg MVK-HIS as substrate in a 200 µl reaction buffer (20 mM Tris-HCl pH 7.5, 10 mM $MgCl_2$, 5 mM EGTA, 100 mM NaCl, and 1 mM DTT, 2 mM ATP) for 30 minutes at 30 °C. In-solution trypsin digestion of the 25 µl reaction was performed at 37 °C O/N and 1 µg protein was loaded to identify phosphorylation sites by Bruker timsTOF Pro. A 40 minutes chromatographic separation (LC) was performed using Thermo C8 Pepmap 100 trap column and Bruker C18 (75 µm x 250 mm) of 1.6 µm particle size (OD4-25075 C18A) served as the analytical column. MS/MS were acquired within 100–1700 m/z using PASEF (Parallel Accumulation-Serial Fragmentation)[74] 10 frames per 1.27 sec cycle

(total 100–120 MS/MS). Automatic script (Bruker Data Analysis v5.1) was applied to convert RAW data to MGF file. Thermo Scientific Proteome Discoverer v 2.2 software running Sequest HT was used to search *Arabidopsis* proteome within NCBI database. Searches were conducted with tolerance of 50 ppm on the precursor and fragment ion mass tolerance of 0.1 dalton, and fixed modification of carbamidomethylation (C), variable modifications of oxidation (M) and phosphorylation (STY). Two biological replicate experiments were conducted.

Immunoblot assay. Total protein was extracted from 10-day-old *Arabidopsis* seedlings by homogenization in extraction buffer containing 50 mM Tris-HCl pH 7.5, 150 mM NaCl, 10 mM $MgCl_2$, 1 mM EDTA, 1 mM DTT, 0.2 mM PMSF, 10% glycerol, 0.5% Triton-X 100, and 1X protease inhibitor (Sigma-Aldrich) for 4 hours on ice. The samples were centrifuged at 20,000 rcf for 10 minutes at 4 °C, then the extracted total proteins were mix with 5X Laemmli loading buffer containing 10% SDS, 50% glycerol, 0.01% bromophenol blue, 10% beta-mercaptoethanol, 0.3 M Tris-HCl pH 6.8, and heated in boiling water 5 minutes. The total extracted proteins were separated by 12% SDS-PAGE gel and detected by immunoblotting with anti-HA-HRP (Roche, dilution 1:2000).

Metabolomic analysis. Polar and semi-polar metabolites from 10-day-old *Arabidopsis* wild-type and *mvk-1* mutant roots were extracted following protocol[75]. Flash frozen pooled root samples were lyophilized and ground to a fine power with a tissue lyser. 800 µl of methanol/water (80:20) was added to 30 mg of pulverized root tissue, and samples were shaken at 1100 rpm for 1 hour at 21 °C in a Thermomixer. Samples were centrifuged for 5 minutes and the supernatant was transferred to a new vial. All extracts were kept at -80 °C until metabolomic analyses.

Root extracts were analyzed with a high-resolution mass spectrometer (HRMS) Orbitrap Velos (Thermo Fisher Scientific) coupled to a Thermo Vanquish HPLC (Thermo Fisher Scientific) equipped with a heated electrospray ionization (HESI) source (Thermo Fisher Scientific). C18 (Hypersil Gold 150 × 2.1 mm, 3 µm particle size) reversed-phase column (Thermo Fisher Scientific) was used for the liquid chromatography at flow rate of 300 µl/min, while column compartment was maintained at 30 °C. HRMS was performed using Fourier transform mass spectrometry (FTMS) and full-scan mode at high resolving power (60,000 full width at half maximum). A mass range of 50-1000 m/z was acquired for each ionization mode. Samples were analyzed in both negative and positive ionization modes. Experimental blanks consisting of methanol/water (80:20) were injected every ~ 15 samples and used to determine the chromatographic background. A mixture of standards was analyzed every 40 samples to test for mass accuracy of the instrument and for further RT and m/z calibration purposes. One injection of methanol/water (80:20) was analyzed right after the standard mixture to avoid any alleged carry over and it was not used for background determination.

Obtained LC-MS RAW files were processed using MZmine 2 version 2.38[76] (Supplementary Table 3) and a final dataset was exported to a CSV file (Supplementary Table 4). Using MZmine 2, metabolic features were assigned to specific metabolite identities using an in-house LC-MS library which contains over 600 typical metabolites from the primary and secondary metabolism of plants. Metabolite annotations were

based on exact mass and retention time (RT) of the detected features corresponding to a second level of identification as detailed by the metabolomics standards initiative[77]. Metabolite annotation information for LC-MS data is detailed in Supplementary Table 5.

To ensure that interesting candidate metabolites were not thrown out during statistical analysis, peak intensity tables containing both previously annotated and unannotated peaks were submitted for missing data imputation using MetImp1.2 (https://metabolomics.cc.hawaii.edu/software/MetImp/)[78]. Following missing data imputation, statistical analysis of the CSV files was done using MetaboAnalyst 4.0 (https://www.metaboanalyst.ca/)[79]. Data was normalized by median, log transformed, and pareto scaling was applied. Following data preparation, both volcano plot analysis (significance $P < 0.05$, FC > 1.5) and fold change analysis were carried out. Box-and-whisker plots were generated via MetaboAnalyst for further analysis. Fold change values were generated for the 7000 + peaks in the normalized data set. Fold change values for the same peak in the various treatments were grouped and analyzed for interesting patterns and flagged for identification. It was then attempted to identify peaks of notable significance – from both volcano plot and fold change analysis – using the mMass software to correlate m/z values to known metabolites using in-house libraries generated from the PlantCyc database (https://plantcyc.org/)[80]. m/z values were matched to candidate metabolites within 0.02 da.

Bacterial inoculation assay. The bacterial inoculation assay was performed with minor modifications as previously described[34]. 2-week-old *Arabidopsis* seedlings were inoculated in 50 ml of *Pseudomonas syringae pv. tomato* DC3000 Lux (OD_{600} = 0.002) bacterial suspension (0.025% Silwet L-77 in sterile water) for 2 minutes at room temperature. After removing the bacterial solution, the plants were incubated in a growth chamber. The first day after inoculation, the aerial part of seedlings was collected and sterilized with 70% ethanol for 1 minute followed by a rinsing step with sterile water three times. Bacterial growth was visualized and measured under a CCD camera (Photek 216; Photek, Ltd.). The homogenized seedling tissue was diluted from 10^{-2} to 10^{-6} and dropped onto King's B agar plates containing rifampicin and kanamycin for 2 days. The bacterial colony forming units (CFU) were counted and analyzed in GraphPad Prism 7.

Declarations

Competing interests

The authors declare no competing interests.

Author contributions

SH.C. designed and performed most of the experiments and wrote the manuscript. K.T. performed the mass spectrometry and edited the manuscript. D.K. performed bimolecular fluorescence

complementation assay and edited the manuscript. P.H.V. and CH.L. performed enzyme assay. P.P.H., A.R.U. and L.PT. performed metabolite analysis. S.E. analyzed metabolites data. G.S. supervised the study and edited the manuscript.

Acknowledgements

We thank current and former members in Gary Stacey laboratory, especially Jeongmin Choi and Kiwamu Tanaka for generating the EMS mutant population. We thank O. Rahul Patharkar for aiding the data analysis of the Illumina sequencing results. Research was supported by the National Institute of General Medical Sciences of the National Institutes of Health (grant no. R01GM121445), the Next-Generation BioGreen 21 Program Systems and Synthetic Agrobiotech Center, Rural Development Administration, Republic of Korea (grant no. PJ01325403) and through the 3rd call of the ERA-NET for Coordinating Action in Plant Sciences, with funding from the US National Science Foundation (grant 1826803). Metabolic analysis was performed using EMSL (grid.436923.9), a DOE Office of Science User Facility sponsored by the Office of Biological and Environmental Research.

References

1. Istvan, E.S. & Deisenhofer, J. Structural mechanism for statin inhibition of HMG-CoA reductase. *Science* **292**, 1160–1164 (2001).
2. Goldstein, J.L. & Brown, M.S. Regulation of the mevalonate pathway. *Nature* **343**, 425–430 (1990).
3. Buhaescu, I. & Izzedine, H. Mevalonate pathway: a review of clinical and therapeutical implications. *Clin Biochem* **40**, 575–584 (2007).
4. van der Meer, J.W. & Simon, A. The challenge of autoinflammatory syndromes: with an emphasis on hyper-IgD syndrome. *Rheumatology (Oxford)* **55**, ii23-ii29 (2016).
5. Akula, M.K. et al. Control of the innate immune response by the mevalonate pathway. *Nat Immunol* **17**, 922–929 (2016).
6. Parrales, A. et al. DNAJA1 controls the fate of misfolded mutant p53 through the mevalonate pathway. *Nat Cell Biol* **18**, 1233–1243 (2016).
7. Li, J. & Fountain, S.J. Fluvastatin suppresses native and recombinant human P2 × 4 receptor function. *Purinergic Signal* **8**, 311–316 (2012).
8. DeClue, J.E., Vass, W.C., Papageorge, A.G., Lowy, D.R. & Willumsen, B.M. Inhibition of cell growth by lovastatin is independent of ras function. *Cancer Res* **51**, 712–717 (1991).
9. He, J.X. et al. Sterols regulate development and gene expression in Arabidopsis. *Plant Physiol* **131**, 1258–1269 (2003).
10. Liao, P., Hemmerlin, A., Bach, T.J. & Chye, M.L. The potential of the mevalonate pathway for enhanced isoprenoid production. *Biotechnol Adv* **34**, 697–713 (2016).

11. Zhang, H. et al. Dolichol biosynthesis and its effects on the unfolded protein response and abiotic stress resistance in Arabidopsis. *Plant Cell* **20**, 1879–1898 (2008).
12. Crowell, D.N. & Huizinga, D.H. Protein isoprenylation: the fat of the matter. *Trends Plant Sci* **14**, 163–170 (2009).
13. Unsicker, S.B., Kunert, G. & Gershenzon, J. Protective perfumes: the role of vegetative volatiles in plant defense against herbivores. *Curr Opin Plant Biol* **12**, 479–485 (2009).
14. Klayman, D.L. Qinghaosu (artemisinin): an antimalarial drug from China. *Science* **228**, 1049–1055 (1985).
15. Woyengo, T.A., Ramprasath, V.R. & Jones, P.J. Anticancer effects of phytosterols. *Eur J Clin Nutr* **63**, 813–820 (2009).
16. Jin, H., Song, Z. & Nikolau, B.J. Reverse genetic characterization of two paralogous acetoacetyl CoA thiolase genes in Arabidopsis reveals their importance in plant growth and development. *Plant J* **70**, 1015–1032 (2012).
17. Ishiguro, S. et al. The Arabidopsis FLAKY POLLEN1 gene encodes a 3-hydroxy-3-methylglutaryl-coenzyme A synthase required for development of tapetum-specific organelles and fertility of pollen grains. *Plant Cell Physiol* **51**, 896–911 (2010).
18. Ohyama, K., Suzuki, M., Masuda, K., Yoshida, S. & Muranaka, T. Chemical phenotypes of the hmg1 and hmg2 mutants of Arabidopsis demonstrate the in-planta role of HMG-CoA reductase in triterpene biosynthesis. *Chem Pharm Bull (Tokyo)* **55**, 1518–1521 (2007).
19. Suzuki, M. et al. Loss of function of 3-hydroxy-3-methylglutaryl coenzyme A reductase 1 (HMG1) in Arabidopsis leads to dwarfing, early senescence and male sterility, and reduced sterol levels. *The Plant Journal* **37**, 750–761 (2004).
20. Kobayashi, K. et al. LOVASTATIN INSENSITIVE 1, a Novel Pentatricopeptide Repeat Protein, is a Potential Regulatory Factor of Isoprenoid Biosynthesis in Arabidopsis. *Plant and Cell Physiology* **48**, 322–331 (2007).
21. Bach, T.J. & Lichtenthaler, H.K. Inhibition by mevinolin of plant growth, sterol formation and pigment accumulation. *Physiologia Plantarum* **59**, 50–60 (1983).
22. Vranová, E., Coman, D. & Gruissem, W. Network analysis of the MVA and MEP pathways for isoprenoid synthesis. *Annu Rev Plant Biol* **64**, 665–700 (2013).
23. Okada, K. et al. Genetic Evidence for the Role of Isopentenyl Diphosphate Isomerases in the Mevalonate Pathway and Plant Development in Arabidopsis. *Plant and Cell Physiology* **49**, 604–616 (2008).
24. Closa, M. et al. The Arabidopsis thaliana FPP synthase isozymes have overlapping and specific functions in isoprenoid biosynthesis, and complete loss of FPP synthase activity causes early developmental arrest. *Plant J* **63**, 512–525 (2010).
25. Ruiz-Sola, M. et al. A Single Arabidopsis Gene Encodes Two Differentially Targeted Geranylgeranyl Diphosphate Synthase Isoforms. *Plant Physiol* **172**, 1393–1402 (2016).

26. Ranf, S. Sensing of molecular patterns through cell surface immune receptors. *Curr Opin Plant Biol* **38**, 68–77 (2017).
27. Ausubel, F.M. Are innate immune signaling pathways in plants and animals conserved? *Nat Immunol* **6**, 973–979 (2005).
28. Choi, H.W. & Klessig, D.F. DAMPs, MAMPs, and NAMPs in plant innate immunity. *BMC Plant Biol* **16**, 232 (2016).
29. Roux, S.J. & Steinebrunner, I. Extracellular ATP: an unexpected role as a signaler in plants. *Trends Plant Sci* **12**, 522–527 (2007).
30. Choi, J. et al. Identification of a plant receptor for extracellular ATP. *Science* **343**, 290–294 (2014).
31. Jewell, J.B. et al. Extracellular ATP Shapes a Defense-Related Transcriptome Both Independently and along with Other Defense Signaling Pathways. *Plant Physiol* **179**, 1144–1158 (2019).
32. Cho, S.H., Nguyen, C.T., Choi, J. & Stacey, G. Molecular Mechanism of Plant Recognition of Extracellular ATP. *Adv Exp Med Biol* **1051**, 233–253 (2017).
33. Chen, D. et al. Extracellular ATP elicits DORN1-mediated RBOHD phosphorylation to regulate stomatal aperture. *Nature communications* **8**, 2265 (2017).
34. Pham, A.Q., Cho, S.H., Nguyen, C.T. & Stacey, G. Arabidopsis Lectin Receptor Kinase P2K2 is a second plant receptor for extracellular ATP and contributes to innate immunity. *Plant Physiol* (2020).
35. Tanaka, K., Swanson, S.J., Gilroy, S. & Stacey, G. Extracellular nucleotides elicit cytosolic free calcium oscillations in Arabidopsis. *Plant Physiol* **154**, 705–719 (2010).
36. Knight, H., Trewavas, A.J. & Knight, M.R. Cold calcium signaling in Arabidopsis involves two cellular pools and a change in calcium signature after acclimation. *Plant Cell* **8**, 489–503 (1996).
37. Chen, D., Ahsan, N., Thelen, J.J. & Stacey, G. S-Acylation of plant immune receptors mediates immune signaling in plasma membrane nanodomains. *bioRxiv*, 720482 (2019).
38. Hoffmann, G. et al. Mevalonic aciduria–an inborn error of cholesterol and nonsterol isoprene biosynthesis. *N Engl J Med* **314**, 1610–1614 (1986).
39. Porter, J.W. Mevalonate kinase. *Methods Enzymol* **110**, 71–78 (1985).
40. Nyati, P., Rivera-Perez, C. & Noriega, F.G. Negative Feedbacks by Isoprenoids on a Mevalonate Kinase Expressed in the Corpora Allata of Mosquitoes. *PLoS One* **10**, e0143107 (2015).
41. Potter, D. & Miziorko, H.M. Identification of catalytic residues in human mevalonate kinase. *J Biol Chem* **272**, 25449–25454 (1997).
42. Favier, L.A. & Schulert, G.S. Mevalonate kinase deficiency: current perspectives. *Appl Clin Genet* **9**, 101–110 (2016).
43. Choi, J. et al. Extracellular ATP, a danger signal, is recognized by DORN1 in Arabidopsis. *Biochem J* **463**, 429–437 (2014).
44. Benhamman, R. et al. The Arabidopsis Mitogen-Activated Protein Kinase Kinase Kinase 20 (MKKK20) Acts Upstream of MKK3 and MPK18 in Two Separate Signaling Pathways Involved in Root Microtubule Functions. *Frontiers in Plant Science* **8** (2017).

45. Bi, G. & Zhou, J.M. MAP Kinase Signaling Pathways: A Hub of Plant-Microbe Interactions. *Cell Host Microbe* **21**, 270–273 (2017).
46. Bouwmeester, K. et al. The lectin receptor kinase LecRK-I.9 is a novel Phytophthora resistance component and a potential host target for a RXLR effector. *PLoS pathogens* **7**, e1001327 (2011).
47. Bouwmeester, K. et al. The Arabidopsis lectin receptor kinase LecRK-I.9 enhances resistance to Phytophthora infestans in Solanaceous plants. *Plant biotechnology journal* **12**, 10–16 (2014).
48. Balague, C. et al. The Arabidopsis thaliana lectin receptor kinase LecRK-I.9 is required for full resistance to Pseudomonas syringae and affects jasmonate signalling. *Molecular plant pathology* **18**, 937–948 (2017).
49. Tripathi, D., Zhang, T., Koo, A.J., Stacey, G. & Tanaka, K. Extracellular ATP Acts on Jasmonate Signaling to Reinforce Plant Defense. *Plant physiology* **176**, 511–523 (2018).
50. Gouget, A. et al. Lectin receptor kinases participate in protein-protein interactions to mediate plasma membrane-cell wall adhesions in Arabidopsis. *Plant Physiol* **140**, 81–90 (2006).
51. Smith, J.M. et al. Loss of Arabidopsis thaliana Dynamin-Related Protein 2B reveals separation of innate immune signaling pathways. *PLoS Pathog* **10**, e1004578 (2014).
52. Manzano, D. et al. Suppressing Farnesyl Diphosphate Synthase Alters Chloroplast Development and Triggers Sterol-Dependent Induction of Jasmonate- and Fe-Related Responses. *Plant Physiol* **172**, 93–117 (2016).
53. Vlot, A.C., Dempsey, D.A. & Klessig, D.F. Salicylic Acid, a multifaceted hormone to combat disease. *Annu Rev Phytopathol* **47**, 177–206 (2009).
54. Tholl, D. & Lee, S. Terpene Specialized Metabolism in Arabidopsis thaliana. *Arabidopsis Book* **9**, e0143 (2011).
55. Venkateshwaran, M. et al. A role for the mevalonate pathway in early plant symbiotic signaling. *Proc Natl Acad Sci U S A* **112**, 9781–9786 (2015).
56. Zhao, J., Davis, L.C. & Verpoorte, R. Elicitor signal transduction leading to production of plant secondary metabolites. *Biotechnol Adv* **23**, 283–333 (2005).
57. Kevei, Z. et al. 3-hydroxy-3-methylglutaryl coenzyme a reductase 1 interacts with NORK and is crucial for nodulation in Medicago truncatula. *Plant Cell* **19**, 3974–3989 (2007).
58. Govindarajulu, M. et al. GS52 ecto-apyrase plays a critical role during soybean nodulation. *Plant Physiol* **149**, 994–1004 (2009).
59. Tanaka, R.D. et al. Molecular cloning of mevalonate kinase and regulation of its mRNA levels in rat liver. *Proc Natl Acad Sci U S A* **87**, 2872–2876 (1990).
60. Schafer, B.L. et al. Molecular cloning of human mevalonate kinase and identification of a missense mutation in the genetic disease mevalonic aciduria. *J Biol Chem* **267**, 13229–13238 (1992).
61. Riou, C., Tourte, Y., Lacroute, F. & Karst, F. Isolation and characterization of a cDNA encoding Arabidopsis thaliana mevalonate kinase by genetic complementation in yeast. *Gene* **148**, 293–297 (1994).

62. Chen, Q. et al. Molecular Cloning, Characterization, and Functional Analysis of Acetyl-CoA C-Acetyltransferase and Mevalonate Kinase Genes Involved in Terpene Trilactone Biosynthesis from Ginkgo biloba. *Molecules* **22** (2017).
63. Haas, D. & Hoffmann, G.F. Mevalonate kinase deficiencies: from mevalonic aciduria to hyperimmunoglobulinemia D syndrome. *Orphanet J Rare Dis* **1**, 13 (2006).
64. Chivasa, S. et al. Extracellular ATP is a regulator of pathogen defence in plants. *Plant J* **60**, 436–448 (2009).
65. Zeng, Q., Wang, X. & Running, M.P. Dual lipid modification of Arabidopsis Ggamma-subunits is required for efficient plasma membrane targeting. *Plant Physiol* **143**, 1119–1131 (2007).
66. Lefebvre, B. et al. A remorin protein interacts with symbiotic receptors and regulates bacterial infection. *Proc Natl Acad Sci U S A* **107**, 2343–2348 (2010).
67. Clough, S.J. & Bent, A.F. Floral dip: a simplified method for Agrobacterium-mediated transformation of Arabidopsis thaliana. *Plant J* **16**, 735–743 (1998).
68. Schiml, S., Fauser, F. & Puchta, H. CRISPR/Cas-Mediated Site-Specific Mutagenesis in Arabidopsis thaliana Using Cas9 Nucleases and Paired Nickases. *Methods Mol Biol* **1469**, 111–122 (2016).
69. Bolger, A.M., Lohse, M. & Usadel, B. Trimmomatic: a flexible trimmer for Illumina sequence data. *Bioinformatics* **30**, 2114–2120 (2014).
70. Langmead, B. & Salzberg, S.L. Fast gapped-read alignment with Bowtie 2. *Nat Methods* **9**, 357–359 (2012).
71. Li, H. et al. The Sequence Alignment/Map format and SAMtools. *Bioinformatics* **25**, 2078–2079 (2009).
72. Reiter, W.D., Chapple, C. & Somerville, C.R. Mutants of Arabidopsis thaliana with altered cell wall polysaccharide composition. *Plant J* **12**, 335–345 (1997).
73. Yoo, S.D., Cho, Y.H. & Sheen, J. Arabidopsis mesophyll protoplasts: a versatile cell system for transient gene expression analysis. *Nat Protoc* **2**, 1565–1572 (2007).
74. Meier, F. et al. Online Parallel Accumulation-Serial Fragmentation (PASEF) with a Novel Trapped Ion Mobility Mass Spectrometer. *Mol Cell Proteomics* **17**, 2534–2545 (2018).
75. Handakumbura, P.P. et al. Metabotyping as a Stopover in Genome-to-Phenome Mapping. *Sci Rep* **9**, 1858 (2019).
76. Pluskal, T., Castillo, S., Villar-Briones, A. & Oresic, M. MZmine 2: modular framework for processing, visualizing, and analyzing mass spectrometry-based molecular profile data. *BMC Bioinformatics* **11**, 395 (2010).
77. Sumner, L.W. et al. Proposed minimum reporting standards for chemical analysis Chemical Analysis Working Group (CAWG) Metabolomics Standards Initiative (MSI). *Metabolomics* **3**, 211–221 (2007).
78. Wei, R. et al. Missing Value Imputation Approach for Mass Spectrometry-based Metabolomics Data. *Sci Rep* **8**, 663 (2018).

79. Chong, J., Wishart, D.S. & Xia, J. Using MetaboAnalyst 4.0 for Comprehensive and Integrative Metabolomics Data Analysis. *Curr Protoc Bioinformatics* **68**, e86 (2019).

80. Strohalm, M., Kavan, D., Novák, P., Volný, M. & Havlícek, V. mMass 3: a cross-platform software environment for precise analysis of mass spectrometric data. *Anal Chem* **82**, 4648–4651 (2010).

Figures

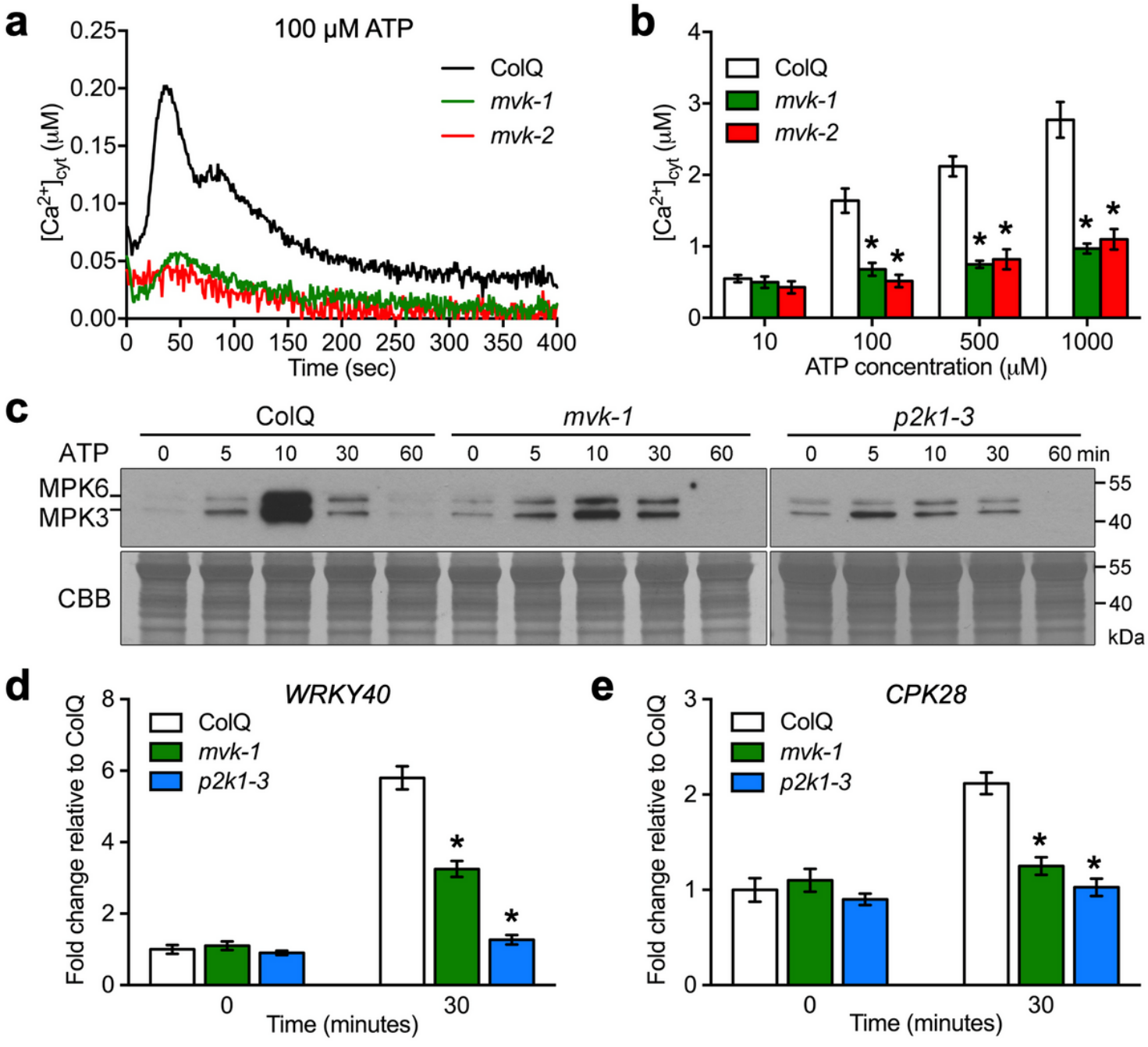

Figure 1

mvk-1 mutants show lower response to extracellular ATP. a The kinetics of the cytoplasmic calcium response to 100 µM ATP for 400 seconds in ColQ, mvk-1, and mvk-2 plants. b The bar graph shows the

integrated calcium response to 10, 100, 500, and 1000 μM of ATP for 400 seconds in ColQ, mvk-1, and mvk-2 mutants. Asterisks indicate significant differences between ColQ, mvk-1, and mvk-2 mutants (means ± SEs, n=12, *P < 0.01). c The mvk-1 mutant exhibits reduced phosphorylation of MPK3 and MPK6 in response to 100 μM of ATP compared to wild-type over a time-course from 0 to 60 min. Phosphorylation of MPK3 and MPK6 was detected using antibody against phospho-p44/p42 mitogen-activated protein kinase. p2k1-3 mutants were used as a negative control. The coomassie brilliant blue (CBB) staining (bottom panel) showed equal loading. d, e Relative expression of WKRY40 and CPK28 in 10-day-old ColQ, mvk-1, and p2k1-3 whole seedlings treated with 100 μM ATP for 30 minutes was performed using qRT-PCR analysis. Gene expression data were normalized using the SAND reference gene. The bar graphs are means of three biological repeats. Asterisks indicate the significant differences compared to ColQ at the same time points (*P < 0.05, Student’s t-test).

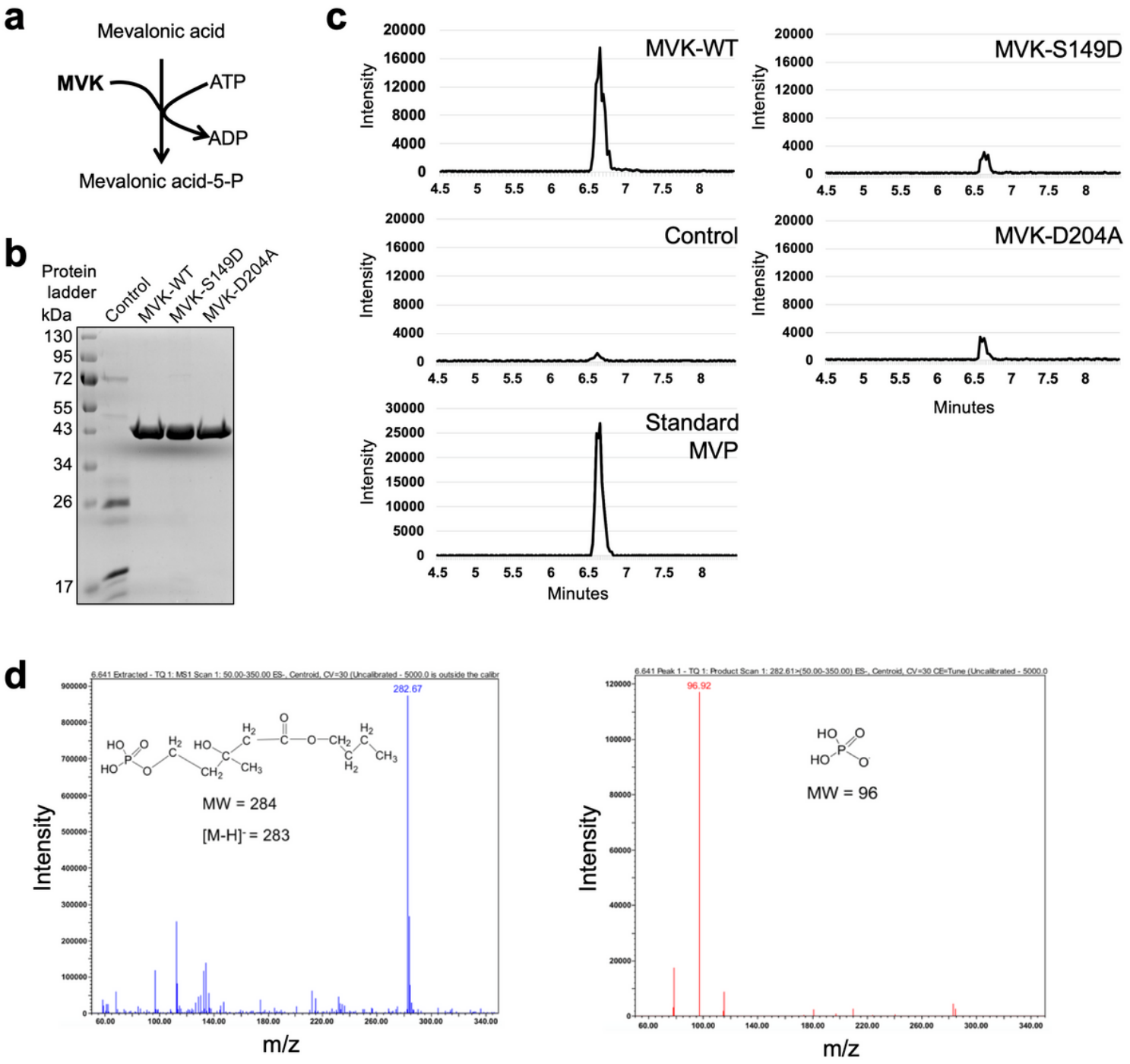

Figure 2

Enzymatic activities of recombinant mevalonate kinase (MVK), and identification of reaction products. a Conversion of mevalonic acid (MVA) into mevalonic acid-5-phosphate (MVP). b SDS-PAGE gel showing His-tag purified proteins expressed in E. coli cells expressing His-tagged MVK-WT, and two dead-versions of MVK (MVK-S149D, and MVK-D204A). As control, proteins were purified from cells carrying empty vector. The protein was measured by coomassie brilliant blue staining. c The ion chromatogram of MVP butyl ester in the samples (MVK-WT, control, MVK-S149D, MVK-D204A, and Standard MVP) quantified by LC-MS/MS analysis (m/z 283→96). MVP+MVK-WT peak (~6.6 minutes) is detected in MVK reaction but not in control (empty vector control cells), and dead-versions of MVK. d The ion spectra of the molecular

ion (m/z 283) (left) and product ions (right) for the analysis of the MVP butyl ester ionized in negative ion mode (ES-).

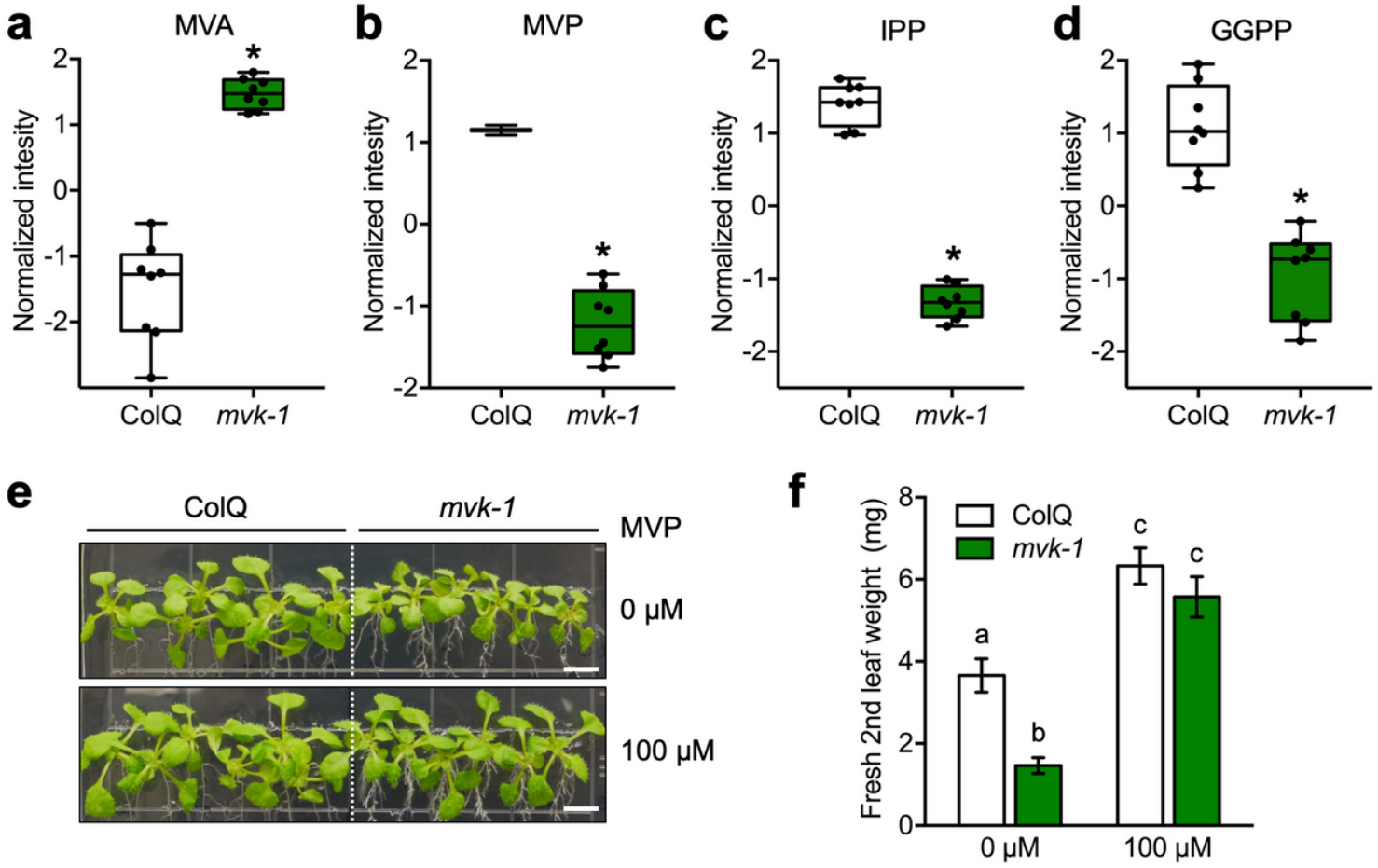

Figure 3

mvk-1 mutant plants show reduced mevalonic acid-5-phosphate (MVP) levels. Exogenous application of MVP partially restores the altered mvk-1 mutant phenotype. a-d Box-and-whisker plots of intermediate compounds in MVA pathway showing their relative abundances. ColQ and mvk-1 mutant root extracts were analyzed with a high-resolution mass spectrometer (HRMS) Orbitrap Velos (Thermo Fisher Scientific) coupled to a Thermo Vanquish HPLC (High Pressure Liquid Chromatographer; Thermo Fisher Scientific). MVA, Mevalonic acid; MVP, Mevalonic acid-5-phosphate; IPP, isopentenyl diphosphate; GGPP, geranylgeranyl diphosphate. Asterisks indicate significant differences between ColQ and mvk-1 (means ± SEs, n=8, *P < 0.05). e 16-day-old ColQ and mvk-1 mutant seedlings grown on medium without or with 100 µM mevalonic acid-5-phosphate (MVP). Scale bars: 0.5 cm. f Fresh second leaf weight of 16-day-old plants (n=21 for ColQ and n=24 for mvk-1). Data represent mean ± SEs from independent experiments. One-way ANOVA analysis was calculated by GraphPad Prism 7. Means with different letters are significantly different (P < 0.05). Experiment was repeated three times with similar results.

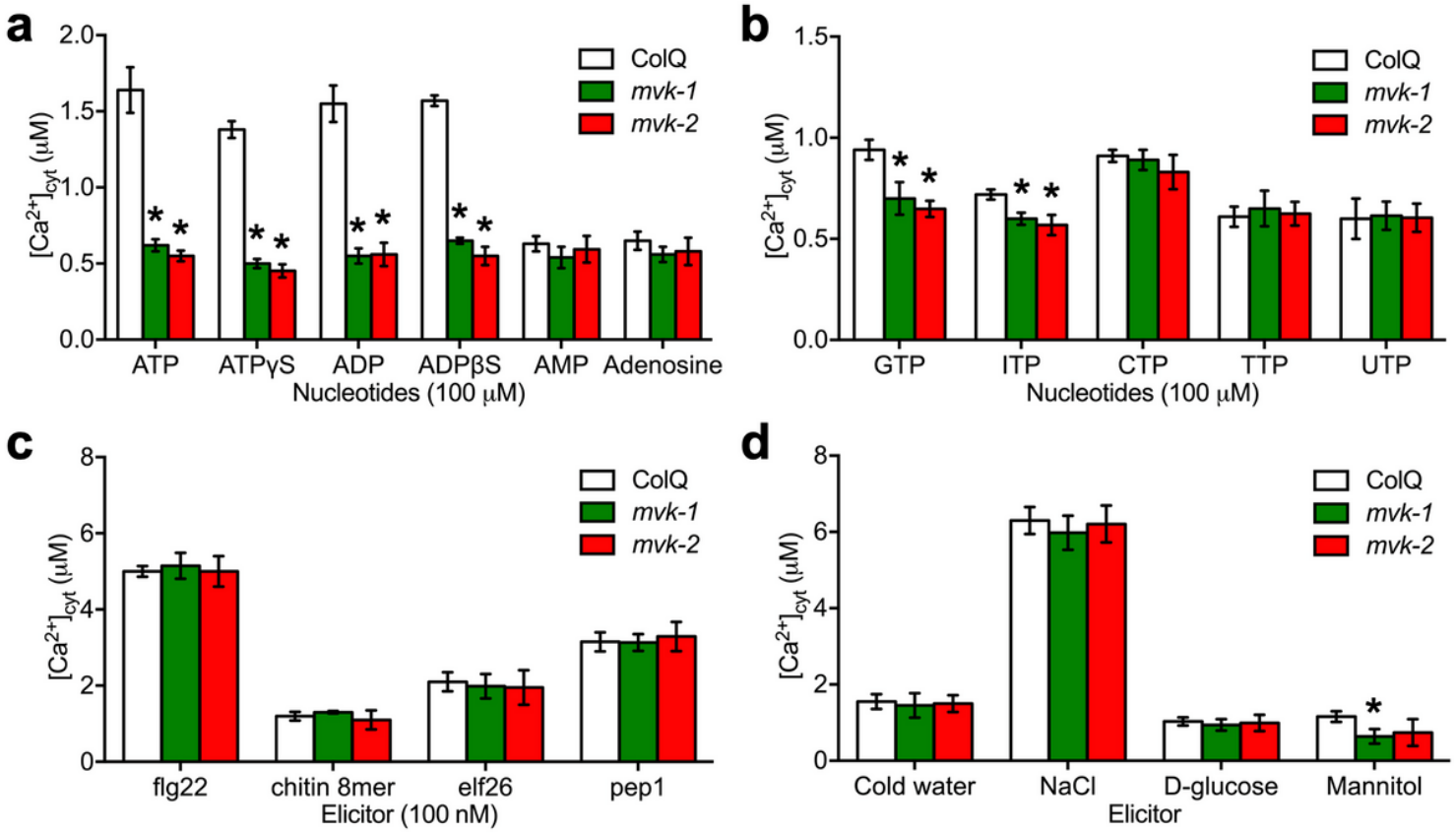

Figure 4

The mvk mutants show defects in the calcium response to various nucleotides. a Calcium responses to adenine nucleotides and non-hydrolysable derivatives in ColQ, mvk-1, and mvk-2 plants. b Calcium responses to other nucleotides in ColQ, mvk-1, and mvk-2 plants. c, d Biotic (100 nM) and abiotic stress reagents (ice-chilled water, 300 mM NaCl, 5% D-glucose, and 300 mM mannitol) induced calcium responses in mvk mutants. All data represented as means ± SEs, n=12 (*P < 0.05).

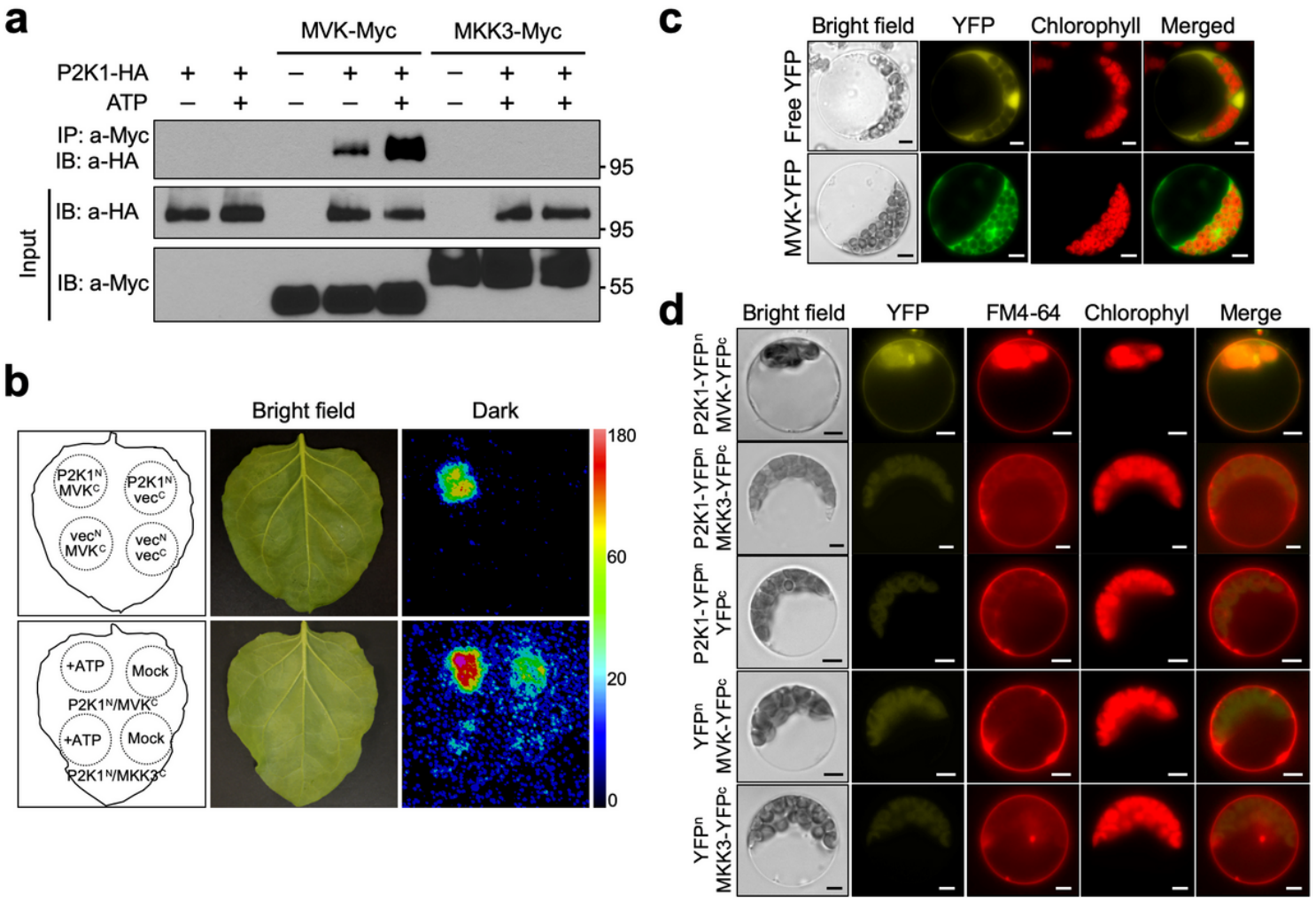

Figure 5

MVK interacts with P2K1 in vivo. a Co-immunoprecipitation of P2K1 and MVK proteins. The indicated constructs were transiently expressed in Nicotiana benthamiana leaves infiltrated with either 200 µM ATP for 30 min (+) or 2 mM MES (pH 5.7) as a control (−). Full-length MKK3 was used as a negative control. Co-IP was performed using anti-HA and anti-Myc antibodies. This experiment was repeated three times with similar results. b Split-luciferase assay image of N. benthamiana leaves co-infiltrated with Agrobacterium strains containing P2K1N/MVKC, P2K1N/vecC, vecN/MVKC, vecN/vecC, and P2K1N/MKK3C (Negative control). Dotted circles indicate leaf panels that were infiltrated with Agrobacterium carrying the respective constructs. +ATP, Leaves infiltrated with 200 µM ATP; Mock, Leaves infiltrated with 2 mM MES (pH 5.7). c Subcellular localization of MVK in Arabidopsis protoplast. Arabidopsis MVK fused to YFP shows cytosolic localization. Free YFP was used as a control. Scale bars: 5 µm. d Biomolecular fluorescence complementation (BiFC) assay in Arabidopsis protoplasts. The indicated constructs were transiently expressed in wild-type protoplasts and the BiFC assay was performed. FM 4-64 was added to stain the plant cell plasma membrane. MKK3 was used as a negative control. Scale bars: 5 µm.

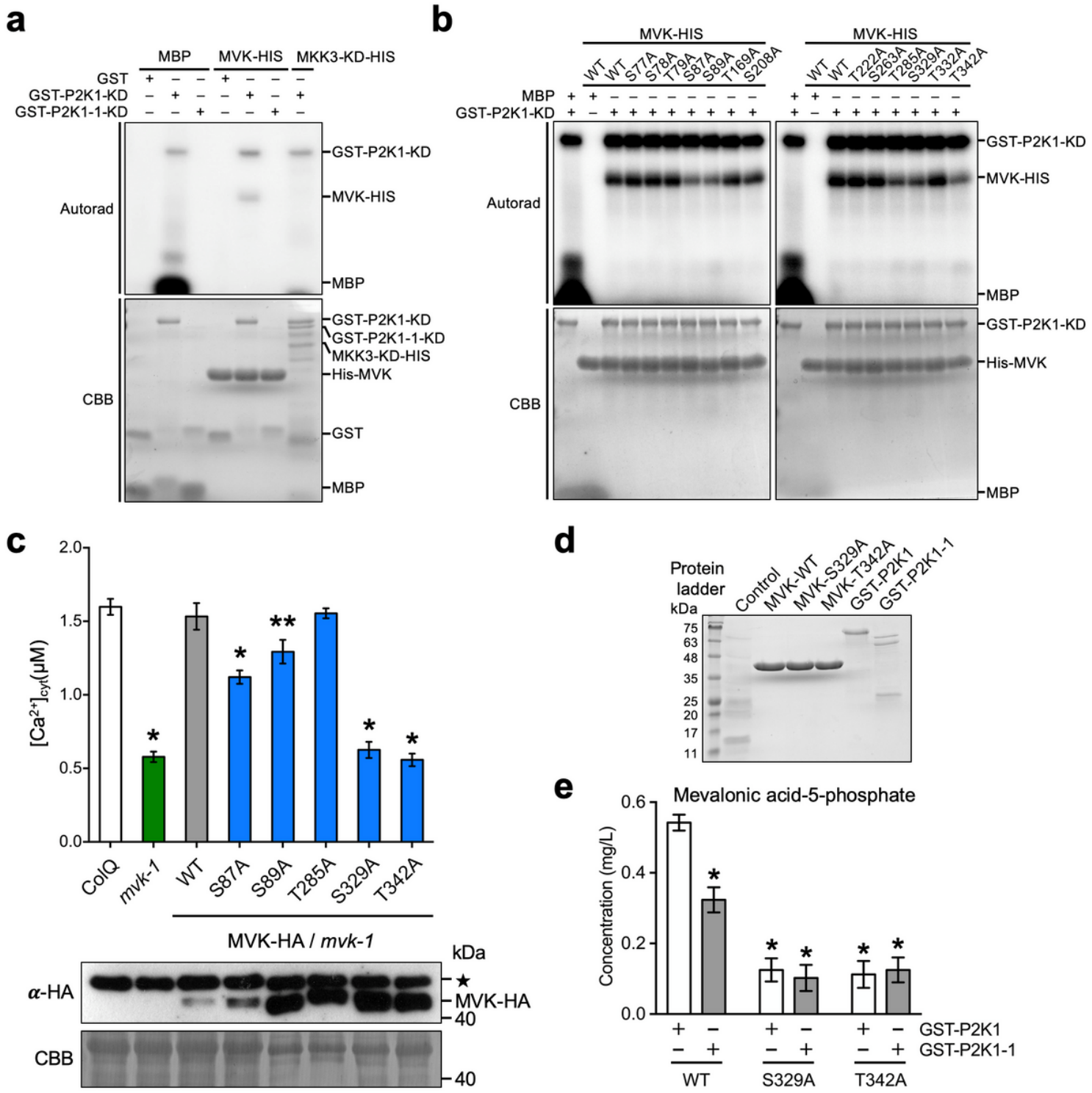

Figure 6

P2K1 phosphorylates MVK in vitro. MVK residues S329 and T342 are required for ATP-triggered calcium production. a P2K1 phosphorylates MVK. Purified MVK-HIS recombinant protein was incubated with GST-P2K1-KD kinase domain, GST-P2K1-1-KD (kinase dead), or GST in an in vitro kinase assay. Autophosphorylation and trans-phosphorylation were measured by incorporation of □-[32P]-ATP. MBP and MKK3-KD-HIS kinase domain were used as positive and negative controls, respectively. Protein loading was visualized by coomassie brilliant blue (CBB) staining. This experiment was repeated three times with

similar results. b P2K1 phosphorylates the MVK and site-directed mutation of P2K1-mediated MVK phosphor sites. Purified MVK-HIS recombinant protein was incubated with GST-P2K1-KD kinase domain in an in vitro kinase assay. Autophosphorylation and trans-phosphorylation were measured by incorporation of □-[32P]-ATP. MBP was used as positive control. Protein loading was visualized by coomassie brilliant blue (CBB) staining. This experiment was repeated three times with similar results. c MVK phosphor sites are required for ATP-triggered calcium production. The indicated constructs were expressed in the mvk-1 mutant background and treated with 100 μM ATP. All data represented as means ± SEs, n=8 (*P < 0.05, **P < 0.001). Total MVK-HA protein was detected by anti-HA immunoblot. Star indicates nonspecific band which was used as a loading control. This experiment was repeated three times with similar results. d Recombinant MVK and P2K1 proteins. SDS-PAGE of HIS and GST tagged proteins isolated from E. coli cells expressing recombinant control (empty vector), MVK-WT-HIS, MVK-S329A-HIS, MVK-T342A-HIS, GST-P2K1-KD, and GST-P2K1-1-KD. Protein loading was visualized by coomassie brilliant blue staining. e Enzymatic activity of P2K1 and MVK-WT, MVK-S329A, and MVK-T342A proteins measured by UPLC-MS/MS. Data are shown as mean ± SEs (n=4, *P < 0.01). This experiment was repeated three times with similar results.

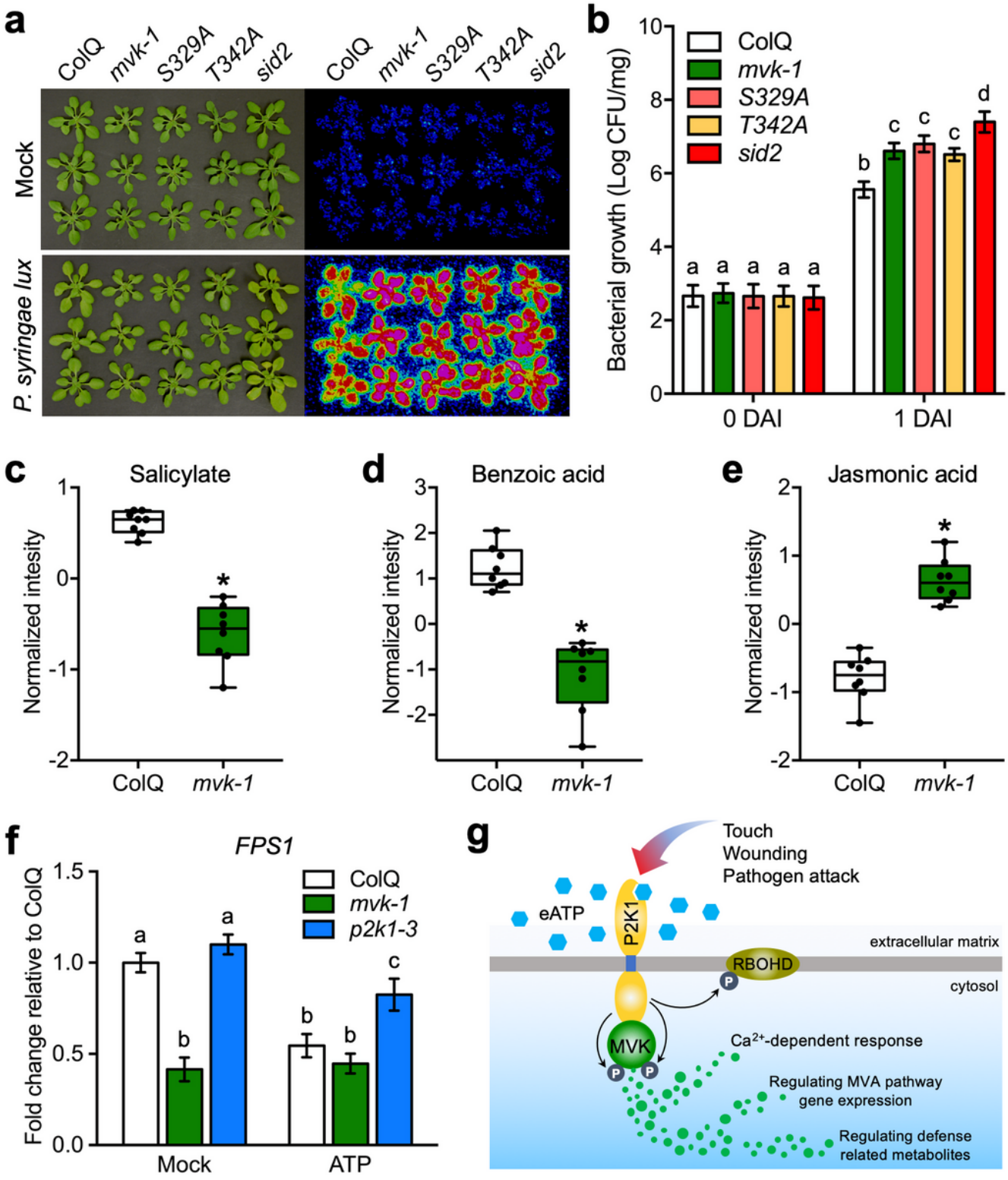

Figure 7

P2K1 mediated MVK phosphorylation at S329 and T342 plays a critical role in plant innate immunity. Altered metabolites and FPS1 gene expression in mvk-1 mutant plants. a, b ColQ and sid2 were used as controls in comparison to mvk-1 mutant plants, as well as mvk-1 plants expressing the S329A, and S342A mutant proteins. 3-week-old plants were flood inoculated with a P. syringae DC3000 lux suspension (OD600 = 0.002) containing 0.025% (v/v) Silwet L-77. a At one day after inoculation, bacteria

invasion was detected by CCD camera. b Bacterial colonization was determined by plate counting (n=12). Data represent mean ± SEs from independent experiments. Two-way ANOVA with Tukey's multiple comparisons analysis were calculated by GraphPad Prism 7. Means with different letters are significantly different ($P < 0.05$). This experiment was repeated three times with similar results. c-e Box-and-whisker plots of significant metabolites showing their relative abundances in ColQ and mvk-1 plants. Root extracts were analyzed with a high-resolution mass spectrometer (HRMS) Orbitrap Velos coupled to a Thermo Vanquish HPLC. Asterisks indicate significant differences between ColQ and mvk-1 (means ± SEs, n=8, *$P < 0.05$). f FPS1 gene expression pattern in response to ATP. 10-day-old ColQ, mvk-1, and p2k1-3 whole seedlings were treated with 2 mM MES (mock) and 100 μM ATP for 60 minutes, then qRT-PCR analysis was performed. Expression of FPS1 was normalized using SAND reference gene. The results are relative to expression levels of mock treated plants (set as 1). Data represent mean ± SEs from independent experiments. One-way ANOVA analysis was calculated by GraphPad Prism 7. Means with different letters are significantly different ($P < 0.05$). This experiment was repeated three times with similar results. g Model illustrating the proposed role of MVK in the extracellular ATP signalling pathway. When extracellular ATP bind to P2K1, MVK is phosphorylated and activated by P2K1 and in turn regulates Ca2+-dependent response, MVA pathway gene expression, and defense related metabolites. RBOHD is also phosphorylated by P2K133.

Supplementary Files

This is a list of supplementary files associated with this preprint. Click to download.

- SungHwanChoSupplementaryTable1.xlsx
- Supplementarytable2SungHwanCho.pdf
- Supplementarytable3SungHwanCho.pdf
- SungHwanChoSupplementaryTable4.xlsx
- SungHwanChoSupplementaryTable5.xlsx
- FigS1.png
- FigS2.png
- FigS3.png
- FigS4.png
- FigS5.png
- FigS6.png
- FigS7.png